Accepted Manuscript

Discovery of new potent dual sigma receptor/GluN2b ligands with antioxidant property as neuroprotective agents

Daniele Zampieri, Sara Fortuna, Antonella Calabretti, Maurizio Romano, Renzo Menegazzi, Dirk Schepmann, Bernhard Wünsch, Simona Collina, Davide Zanon, Maria Grazia Mamolo

PII: S0223-5234(19)30633-6

DOI: https://doi.org/10.1016/j.ejmech.2019.07.012

Reference: EJMECH 11509

To appear in: *European Journal of Medicinal Chemistry*

Received Date: 14 May 2019

Revised Date: 20 June 2019

Accepted Date: 4 July 2019

Please cite this article as: D. Zampieri, S. Fortuna, A. Calabretti, M. Romano, R. Menegazzi, D. Schepmann, B. Wünsch, S. Collina, D. Zanon, M.G. Mamolo, Discovery of new potent dual sigma receptor/GluN2b ligands with antioxidant property as neuroprotective agents, *European Journal of Medicinal Chemistry* (2019), doi: https://doi.org/10.1016/j.ejmech.2019.07.012.

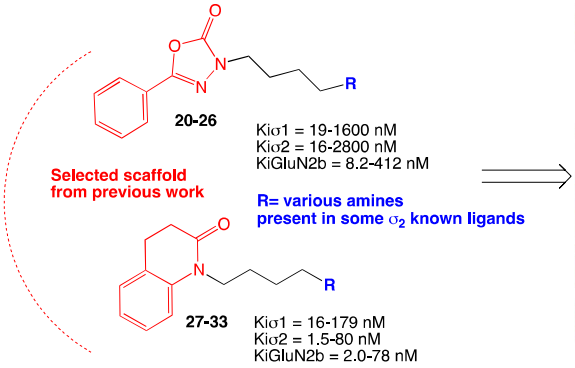

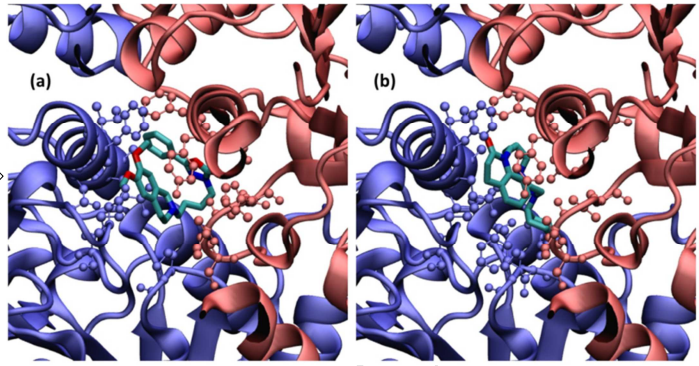

(a) Docking of compounds **24** (KiGluN2b = 27 nM) and (b) **28** (KiGluN2b = 2.0 nM) into the binding site of GluN2b subunit.

Discovery of new potent dual sigma receptor/GluN2b ligands with antioxidant property as neuroprotective agents.

Daniele Zampieri[a*], Sara Fortuna[a*], Antonella Calabretti[a], Maurizio Romano[b], Renzo Menegazzi[b], Dirk Schepmann[c], Bernhard Wünsch[c], Simona Collina[d], Davide Zanon[e], Maria Grazia Mamolo[a].

[a]*Department of Chemistry and Pharmaceutical Sciences, Piazzale Europa 1- Via Giorgieri 1, University of Trieste, 34127 Trieste, Italy.*

[b]*Department of Life Sciences, Via Valerio 28/1, University of Trieste, 34127 Trieste, Italy.*

[c]*Institut für Pharmazeutische und Medizinische Chemie Westfälische Wilhelms-Universität Münster, Corrensstraße 48, D-48149 Münster, Germany.*

[d]*Department of Drug Sciences, Medicinal Chemistry and Pharmaceutical Technology Section, Viale Taramelli 6 and 12, University of Pavia, 27100 Pavia, Italy.*

[e]*Pharmacy and Clinical Pharmacology Department Institute for Maternal and Child Health IRCCS Burlo Garofolo Via dell'Istria 65/1, 34137 Trieste, Italy.*

* *Corresponding authors:* Prof. Daniele Zampieri; tel: +390405587858; email: dzampieri@units.it; Prof. Sara Fortuna (molecular simulations); email: s.fortuna@units.it; web: http://sarafortuna.eu/

Keywords

Sigma receptors (σRs), GluN2B receptor, pan-affinity, molecular dynamics, antioxidant activity, neuroprotective activity.

Abstract

Among several potential applications, sigma receptors (σRs) can be used as neuroprotective agents, antiamnesic, antipsychotics and against other neurodegenerative disorders. On the other hands, antagonists of the GluN2b-subunit-containing-N-methyl-D-aspartate (NMDA) receptors are of major interest for the same purpose, being this subunit expressed in specific areas of the central nervous system and responsible for the excitatory regulation of nerve cells. Under these premises, we have synthesized and biologically tested novel hybrid derivatives obtained from the combination of phenyloxadiazolone and dihydroquinolinone scaffolds with different amine moieties, peculiar of σ2R ligands. Most of the new ligands exhibited a pan-affinity towards both σR subtypes and high affinity against GluN2b subunit. The most promising compounds belong to the dihydroquinolinone series, with the best affinity profile for the cyclohexylpiperazine derivative **28**. Investigation on their biological activity showed that the new compounds were able to protect SH-SY5Y cells against oxidative stress induced by hydrogen peroxide treatment. These results proved that our dual σR/GluN2b ligands have beneficial effects in a model of neuronal oxidative stress and can represent strong candidate pharmacotherapeutic agents for minimizing oxidative stress-induced neuronal injuries.

1. Introduction

After initial cloning in 1996, the Sigma 1 receptor gene (σ1R) was found to be evolutionarily conserved. Its encoded protein consists of 223 amino acids with a predicted molecular weight of 25.3 kDa [1,2, 3], and was crystallized in 2016, revealing a trimeric protein organization [4]. The σ1R subtype is particularly enriched in mitochondrion-associated endoplasmic reticulum membranes (MAM) of neuronal and peripheral cells, such as myocardiocytes and hepatocytes. They can also translocate to the plasma membrane or ER-membrane and regulate other proteins, as well as act as chaperone, modulating different ionic channels (Ca^{2+}, K^{+}, Na^{+}, Cl^{-}) via an IP_3-indipendent mechanism [5,6]. The σ1Rs exert a modulatory role on many transduction systems such as muscarinic, dopaminergic, serotoninergic and on the NMDA-stimulated neurotransmitter's release [7].

Regarding functions, the σ1Rs have neuroprotective and antiamnesic activities [8], and are involved in modulation of opioid analgesia [9] and drug addiction [10]. Alongside, σ1 antagonists seem to be effective against the negative manifestations of schizophrenia, without producing extrapyramidal side effects [11,12].

In addition, several studies suggest a role for σ1R in tumor biology, supported by the observation that its expression is increased in some cancers and by the growth inhibiting effects of putative antagonists [13].

In 2017, after 40 years from the discovery of σRs [14], the σ2R subtype has been purified and identified as the transmembrane protein-97 (TMEM97), also named Meningioma-associated protein 30 (MAC-30) [15]. It is a conserved protein consisting of 176 amino acids with a predicted molecular weight of 21 kDa, localized to the plasma membrane, endoplasmic reticulum and nuclei.

TMEM97/σ2R is a member of the insulin-like growth factor-binding protein family, and plays a role in cholesterol homeostasis regulation [16]. This role was then further confirmed by a study reporting how the interaction of TMEM97 with the progesterone receptor membrane component-1 and the LDL receptor, was critical for the internalization of LDLs [17, 18].

TMEM97/σ2R is implicated in several cellular processes, such as proliferation, signal transduction, apoptosis and autophagy. In fact, siramesine (SRMS), a specific σ2R agonist, was shown to trigger apoptosis by caspase activation, autophagy by mTOR kinase inhibition, as well as cell-cycle alterations [19].

The σ2R is widely distributed in brain and, particularly, in cerebellum, red nucleus and substantia nigra. Therefore, it is a potential target for the treatment of motor control in movement disorders

and for counteracting the extrapyramidal side effects produced by neuroleptics drugs [20]. Interestingly, not only σ1R antagonists [21], but also σ2R agonists are involved in neuropathic pain [22].

In addition, TMEM97/σ2R seems to have also an impact on tumor growth. Except for pancreatic and renal cancers [23], it is overexpressed in several types of cancers, and consequently associated with tumor progression, poor survival and recurrence [24-29].

These observations have suggested the use of σ2 receptor agonists as potential therapeutics for the treatment of cancer and that TMEM97 could be used as potential prognostic biomarkers of non-small cell lung carcinoma (NSCLC), squamous cell lung carcinoma (SQCLC), ovarian and breast cancers [30].

On the other hand, the N-methyl-D-aspartate receptors (NMDARs) are a heterogeneous class of glutamate-responsive ion-channel receptors located in the post-synaptic membranes of most excitatory synapses [31]. These proteins, along with AMPA (2-amino-3(3-hydroxy-5-methylisoxazol-4-yl)propionate) and Kainate, belong to the ionotropic (S)-Glutamate receptors (iGluRs) family. Structurally, NMDARs are heterotetrameric complexes with four distinct components derived from three related families, named GluN1, GluN2 and GluN3. In particular, NMDARs consist of two GluN1 and two GluN2 subunits [32], but one GluN1 can be replaced by one GluN3 subunit [33].

A further level of structural and functional complexity stems from the observation that up to 8 isoforms can be generated by alternative splicing of the single GluN1 gene (GluN1a-h), while the GluN2 type is encoded by four genes (GluN2a-d) and the GluN3 by two genes (GluN3a-b) [34].

Overstimulation of NMDARs, as a consequence of (S)-glutamate excess and the subsequent uncontrolled neuronal influx of Ca^{2+} ions, causes excitotoxicity and triggers cell death by apoptosis. Importantly, this phenomenon is responsible for the onset and progression of several neurodegenerative diseases [35].

Likewise, for σRs, the NMDARs play key roles in synaptic transmission, synaptic plasticity, neuronal development, learning, memory and other physiological and pathological processes [36, 37]. Hence, antagonists of NMDAR (and, in particular, of the GluN2 subunits) are of interest as potential neuroprotective drugs to treat several central nervous system (CNS) disorders. While high-affinity NMDAR-inhibitors include psychotomimetic and neurotoxic agents (such as phencyclidine and (+)-MK-801), the low-affinity NMDAR- antagonists (such as memantine and amantadine) represent a class of drugs without such effects already used clinically to treat Alzheimer's and Parkinson's diseases.

Ifenprodil (**1**, Figure 1A) [38] is one of the prototypical allosteric inhibitors which interacts only with the GluN2b-containing NMDARs [39].

In 2011, the binding site of the selective GluN2b ligands was characterized and it was found to be at the interface between the GluN1 and GluN2b subunits [40]. In 2014, the full heterotetrameric NMDAR protein has been co-crystallized with Ifenprodil **1** (4-[2-(4-benzylpiperidin-1-yl)-1-hydroxypropyl]phenol) [41] and an its partial agonist analogue Ro-25-6981 **2** (Figure 1A) [42].

Under these premises, a multi-targets drugs (MTD) approach, such as dual σR/GluN2bR modulators, can be beneficial for the enhancement of neuroprotection to treat several CNS disorders.

In our past work, we have synthesized some new 1-(4-(aryl(methyl)amino)butyl)-heterocyclic derivatives [43], showing high affinity and selectivity towards the σ1R subtype. Their *K*i-values were in the low nanomolar range (0.95 nM-3 μM), but demonstrated a very low affinity for the σ2R subtype (*K*i = 42 nM-3μM) (Figure 1B).

Aiming to improve the σ2R affinity of our previously synthesized compounds, and concurrently discover novel GluN2bR ligands, we designed and synthesized new molecules obtained by retaining two of the most representative scaffolds of the previous series and by jointly replacing the N-benzylmethylamine (and the 4-chlorobenzyl analogue) fragment with other amine moieties present in some well-known σ2R ligands.

The preserved structures were the 5-phenyl-1,3,4-oxadiazole-2(3*H*)-one (**3a,b**) and the dihydroquinolin-2(1*H*)-one (**3c,d** highlighted in red, Figure 1B) scaffolds, which provided the best compromise between σ1 profile and ease of synthesis.

The selected amine moieties were the spiro[isobenzofuran-1,4'-piperidine] (**4,** SRMS), N-cyclohexylpiperazine (**5,** PB-28), N-(4-fluorophenyl)piperazine (**6,** SN-79), N-(pyridin-2-yl)-piperazine (**7**), 6,7-dimethoxy-3,4-dihydroisoquinoline (**8,** RHM-1), 7-nitro-3,4-dihydroisoquinoline (**9**) and 2,4-dimethylbenzyl-N-methylamine (**10**, our SRMS analogue, named DZ-24) [44] (highlighted in blue, Figure 1C).

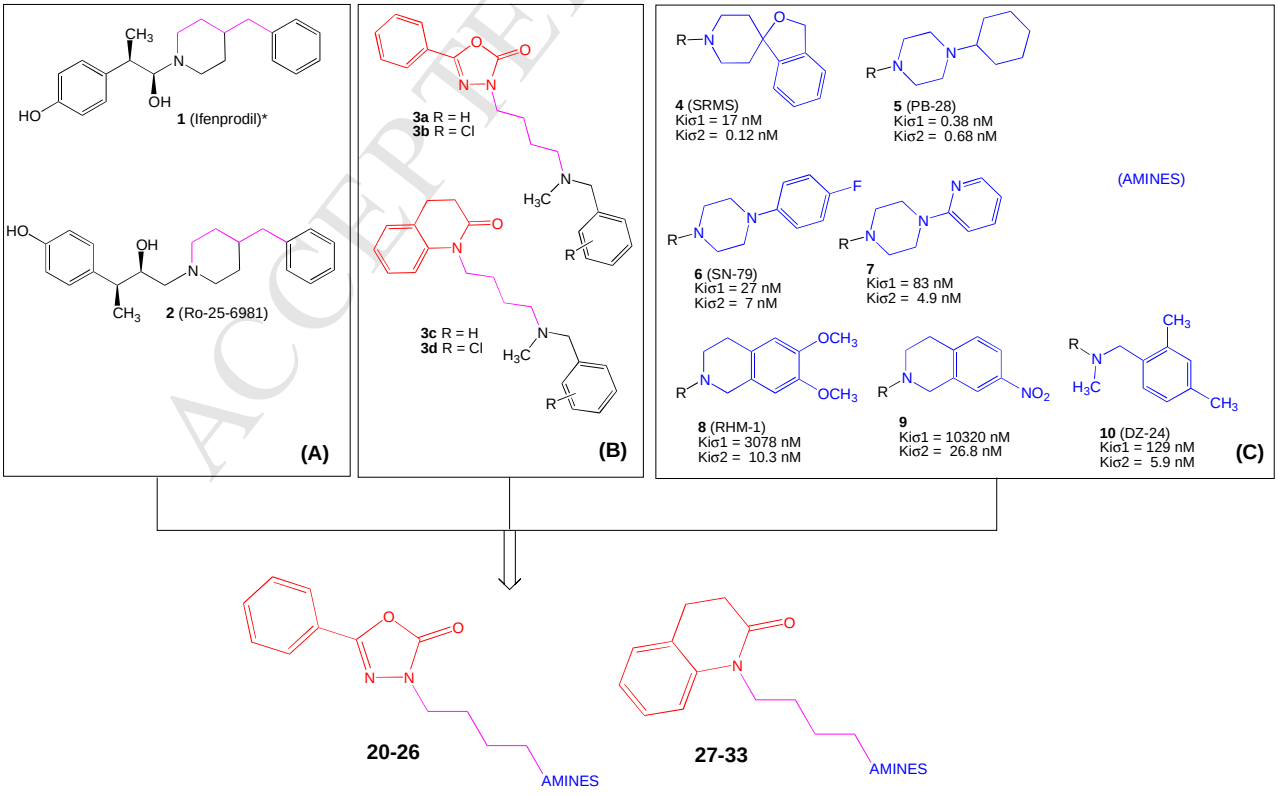

Figure 1. Design of target compounds as dual σR/GluN2b ligands. (A) Structure of two known references GluN2b ligands. *Ifenprodil represents the racemic *erythro* diastereomer. (B) Selected scaffold from our previous work. (C) Selected amine scaffolds from well-known σ2 ligands and their *K*iσ1 and *K*iσ2 values (nM).

As already pointed out, the rigid piperidine(methyl) central scaffold of ifenprodil, can be replaced by the more flexible butylamine spacer (highlight in purple, Figure 1A), without altering the affinity [45]. The same structural central motif is often present in many σR ligands, as previously reported [43, 46]. Moreover, the selectivity σ2/σ1 can be modulated by substitution of one of the two aromatic side scaffolds. Indeed, the substitution of a simple phenyl ring with the dimethylphenyl ring causes a marked shift of the selectivity from σ1R to σ2R subtype. Taking this into account, we planned to synthesize the new hybrid molecules **20-33 (Scheme 1)**.

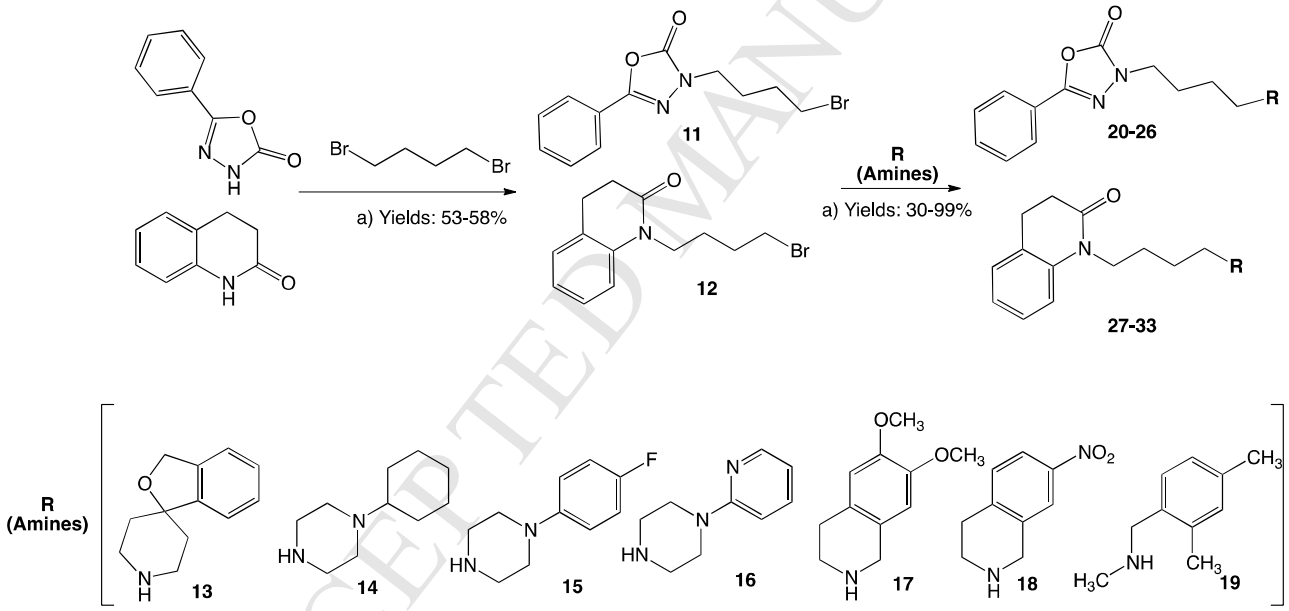

Scheme 1. Synthesis of title compounds **20-33**. Reagents and conditions: a) K_2CO_3, KI (cat) or $CsCO_3$, TBAB (cat), ACN, reflux; b) Amine **13-19**, K_2CO_3, KI (cat), ACN, reflux.

2. Results and discussion

2.1 Chemistry

On one hand, the synthesis of title compounds **20-26** was carried out from 5-phenyl-1,3,4-oxadiazole-2(3*H*)-one, obtained from the cyclization of benzoic acid hydrazide with triphosgene [43]. On the other, derivatives **27-33** were obtained from the commercially available 3,4-dihydroquinolin-2(1*H*)-one. These two precursors were made react with an excess of 1,4-

dibromobutane in basic media, in order to obtain the intermediate compounds **11** and **12**, respectively. The latter underwent nucleophilic substitution, in the presence of potassium carbonate and KI as catalyst, with the corresponding amines **13-19**, to afford the final compounds **20-33** in good yields. The amines **13-19** were commercially available with the exception of 7-nitro-1,2,3,4-tetrahydroisoquinoline **18** and 1-(2,4-dimethylphenyl)-*N*-methylmethanamine **19**. The first was prepared by nitration of 1,2,3,4-tetrahydroisoquinoline with H_2SO_4/KNO_3 and then converted into hydrochloride salt. The latter was prepared via a classical indirect reductive amination involving 2,4-dimethylbenzaldehyde and methylamine to form the corresponding Schiff base, which was subsequently reduced with $NaBH_4$ to afford the desired intermediate **19**.

2.2 Receptor affinity, selectivity and SAR exploration

The synthesized compounds **20-33** were investigated for their potential affinity towards σ1R, σ2R and GluN2b subunit containing NMDA receptors. Guinea pig brain and rat liver homogenates were used as sources for the σ1R and σ2R assays, respectively. While the [^{3}H]-(+)-pentazocine was utilized as selective σ1R radioligand, the [^{3}H]-1,3-di(o-tolyl)guanidine was utilized as nonselective σ2R radioligand, in the presence of nontritiated (+)-pentazocine (to selectively occupy the σ1Rs). The affinity towards GluN2b subunit was performed in a radioligand binding assay developed by the Authors [47]. Briefly, L(tk-) cells stably transfected with a vector containing the genetic information for the GluN1a and GluN2B subunits of the NMDA receptor provided the receptor material. Using membrane preparations of these cells and [^{3}H]-labeled ifenprodil as radioligand, the affinity of compounds was determined in a competition assay. The data are collected in Table 1.

Table 1. GluN2b, σ1R and σ2R affinity and the corresponding selectivity ratios of title compounds **20-33** and reference compounds. The blood brain barrier (BBB) score of title compounds is related to the ability to diffuse into the CNS.

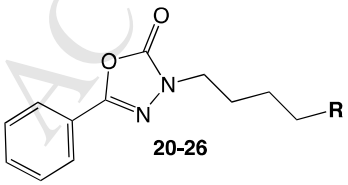

20-26

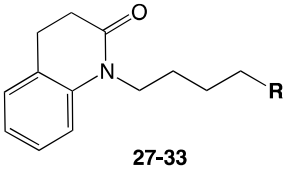

27-33

Cpd	R	*Ki* [nM][a]			Selectivity ratio		BBB score
		σ1	σ 2	GluN2b	σ1/σ2	σ2/GluN2b	
20	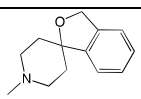	19 ± 8	16 ± 5	8.2 ± 3	1.2	2.0	4.38
21	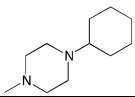	35 ± 5	93 ± 35	23 ± 7	0.37	4.0	4.25

22	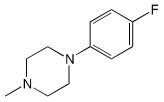	383	686	68 ± 7	0.57	10	3.98
23	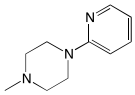	944	2800	226	0.33	12.4	4.84
24	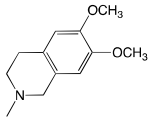	1600	864	27 ± 6	1.8	32	4.35
25	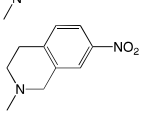	829	383	412	2.2	0.9	4.07
26	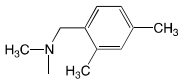	20 ± 9	21 ± 10	26 ± 2	0.95	0.8	3.34
27	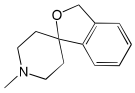	18 ± 4	34 ± 15	5.0 ± 0.9	0.5	6.8	4.57
28	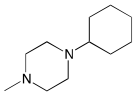	21 ± 2	1.5 ± 1.1	2.0 ± 0.2	14	0.75	4.22
29	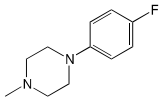	16 ± 7	21 ± 11	8.1 ± 3	0.76	2.6	3.91
30	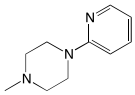	120 ± 19	73 ± 22	78 ± 6	1.6	0.9	5.44
31	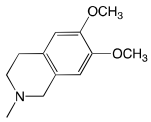	116 ± 32	45 ± 22	12 ± 5	2.6	3.7	4.91
32	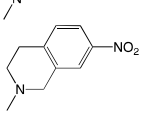	179	80 ± 3	58 ± 10	2.2	1.4	4.60
33	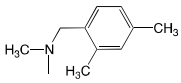	60 ± 18	32 ± 9	5.0 ± 1.4	1.9	6.4	2.98
Ifenprodil	-	125 ± 24	98 ± 34	10 ± 0.7	1.3	9.8	4.41
Haloperidol	-	6.3 ± 1.6	78 ± 2.3	nt	0.08	nc	5.54
DTG	-	89 ± 29	57 ± 18	nt	1.5	nc	nc

[a]Only the most potent compounds (*K*i < 150 nM) were tested in triplicate; [b] 0-2 don't cross BBB, 2-5 may cross BBB, 5-6 effectively cross BBB; nt: not tested; nc: not calculated.

Although the phenyloxadiazolone series **20-26** has provided higher *K*i values than the corresponding dihydroquinolinone series **27-33**, some derivatives have proved to be rather interesting by confirming some known evidences. Among them, compounds **20**, **21** and **26** showed high σ1R affinity, comparable to our previously parent derivatives. In fact, the *K*iσ1 values were ranging from 19 to 35 nM (5.2–18.7 nM for **3a,b**), and the *K*iσ2 values were 16 nM, 23 nM and 21 nM, respectively (*versus K*iσ2R values ranging from 110 to 315 nM for **3a-d** [43]). Therefore, these ligands showed an increased affinity towards σ2R subtype.

These results are supported by the presence of the bulky spiro[isobenzofuran-1,4'-piperidine], cyclohexylpiperazine and 2,4-dimethylbenzyl-N-methylamine moieties, confirming their importance for the σ2R affinity/selectivity, with respect to benzyl-N-methylamine or 4-chlorobenzyl-N-methylamine scaffold of our previously compounds **3a-d**. Interestingly, compound **20** showed the best inhibition value towards GluN2b subunit (*K*i = 8.2 nM), even better than the reference drug ifenprodil. On the contrary, the 6,7-dimethoxy-3,4-dihydroisoquinoline derivative **24** exhibited the best selectivity profile, with a 32-fold preference for GluN2b receptor (*K*i = 27 nM) over σ2R (*K*i = 864 nM) and could be considered the *hit* compound to design new selective GluN2bR ligands.

Regarding the homologous subseries of dihydroquinolinones **27-33**, all the compounds showed a moderate to high σR pan-affinity, with the best result of the entire series against σ1R, for the 4-fluorophenylpiperazinyl derivative **29** (*K*iσ1R = 16 nM). Conversely, the cyclohexylpiperazinyl derivative **28** showed the best affinity against σ2R (*K*i = 1.5 nM) and GluN2bR (*K*i = 2 nM), along with a favourable σR selectivity ratio (σ1/σ2 = 14). Finally, the spiro[isobenzofuran-1,4'-piperidine] **27** and the 2,4-dimethylbenzyl-N-methylamino **33** derivatives resulted to be twice as powerful as ifenprodil over GluN2bR (*K*i = 5 nM) and demonstrated a comparable selectivity (6.4 fold *versus* 9.8).

2.3 *In-silico* properties

In order to predict their drug likeness and the ability to reach the CNS, the compounds **20-33** were also *in silico* evaluated for their physiochemical and pharmacokinetics parameter (ADME). For this latter purpose, we used the following molecular descriptors: molecular weight (MW); acid dissociation constant (pKa); number of H-bond donors (HBD); calculated partition coefficient (clogP); calculated distribution coefficient (clogD); and topological polar surface area (TPSA). These features have been considered following the algorithm of central nervous system multiparameter optimization (CNS MPO), developed by Wager *et al.* [48] which attributes a value between 0 and 1 for each aforementioned parameter. The collective score, ranging from 0 to 6, gives an indication of the drug's ability in crossing the BBB and precisely: i) 0-2 the compound does not cross the BBB; ii) 2-4 the compound can reach the CNS; iii) 5-6 the compound surely crosses the BBB. We evaluate all the final scores of the entire series **20-33,** in comparison with ifenprodil, siramesine and haloperidol as reference drugs (Table SI1). All the synthetized compounds showed a good score in the median range (2-5), and the derivative **30** was the best scored with a value > 5. Furthermore, all the compounds do not violate more than one score of the extended version of Lipinski's rule of five (RO5: MW≤ 500; HBA ≤ 10 and HBD ≤ 5, respectively;

logP and logS ≤ 5; TPSA ≤ 140 Å) [49], confirming their good drug likeness and the potential ability to be orally active in humans. Altogether these results support the hypothesis that all the derivatives should be able to cross the BBB and reach the CNS.

Table 2. *In silico* CNS MPO of main pharmacokinetic parameters, and relative scores, of compounds **20-33** to define their ability in crossing the BBB. (Marvinsketch® Chemaxon).

Cpd	MW[a] (KDa)	Score MW	HBD[b]	Score HBD	pKa[c]	Score pKa	clogP[d]	Score logP	clogD[e]	Score logD	TPSA[f] (Å)	Score TPSA	Final score BBB[g]	RO5 viol.[h]
20	405.49	0.47	0	1	9.34	0.33	3.84	0.58	1.90	1	54.37	1	4.38	0
21	384.52	0.58	0	1	9.04	0.48	4.13	0.43	2.48	0.76	48.38	1	4.25	0
22	396.46	0.52	0	1	8.28	0.86	4.36	0.32	3.43	0.28	48.38	1	3.98	0
23	379.46	0.60	0	1	8.09	0.95	3.60	0.7	2.82	0.59	61.27	1	4.84	0
24	409.48	0.45	0	1	8.18	0.91	3.93	0.53	3.08	0,46	63.60	1	4.35	0
25	394.42	0.53	0	1	7.79	1	4.19	0.40	3.65	0.17	90.96	0.97	4.07	0
26	365.47	0.67	0	1	9.57	0.21	5.23	0	3.08	0.46	45.14	1	3.34	1
27	390.52	0.55	0	1	9.09	0.45	3.34	0.83	1.64	1	32.78	0.64	4.57	0
28	369.54	0.70	0	1	9.02	0.49	3.62	0.69	2.00	1	26.79	0.34	4.22	0
29	381.49	0.59	0	1	8.03	0.98	3.86	0.57	3.14	0.43	26.79	0.34	3.91	0
30	364.48	0.77	0	1	7.84	1	3.09	0.95	2.51	0.74	39.68	0.98	5.44	0
31	394.51	0.53	0	1	7.93	1	3.43	0.78	2.79	0.60	42.01	1	4.91	0
32	379.45	0.60	0	1	7.53	1	3.68	0.66	3.31	0.34	69.37	1	4.60	0
33	350.50	0.75	0	1	9.27	0.36	4.73	0.13	2.87	0.56	23.55	0.18	2.98	0
Ifenp.	325.45	0.87	2	0.50	9.03	0.48	3.57	0,71	2.30	0.85	43.70	1	4.41	0
SRMS	454.59	0.23	0	1	9.56	0.22	6.58	0	4.43	0	17.40	0	1.45	1
Haloo.	375.87	0.62	1	0.75	8.05	0.97	3.66	0.67	2.93	0.53	40.54	1	5.54	0

[a]Molecular Weight; [b]number of H-bond donors; [c]logarithmic acid dissociation constant of most basic group; [d]calculated logarithmic Octanol/Water repartition; [e]calculated logarithmic distribution coefficient (pH = 7.4); [f]Topological Polar Surface Area; [g]Blood Brain Barrier permeability score (0-6); [h]Lipinski's rule of five (RO5) violations (HBA and cLogS data not shown).

2.4 Molecular modeling

From the obtained results reported in Table 1 we selected two representative compounds: **24**, which showed the best selectivity profile, and **28**, with the highest affinity towards GlN2b, for the molecular dynamic simulations.

We chose the pdb 4PE5 [41] containing the x-ray structure of the rat heterotetrameric NMDA receptor, where the chains A and C correspond to two GluN1a units, while the chains B and D correspond to two GluN2b units. The (R, S)-ifenprodil (4-[(1R,2S)-2-(4-benzylpiperidin-1-yl)-1-hydroxypropyl]phenol) is bound at the interface between chains A/B and C/D. We chose chain A and B as template to reconstruct one single binding site (Supplementary Figure S1a).

Our compounds are expected to bind to the (R, S)-ifenprodil binding site of GluN2B (Supplementary Figure S1b). To test the docking method, we first minimised both target and ligand, then we performed the docking. Autodock led to a first ranked conformation with RMSD 0.902 Å

with respect to the crystal structure and a predicted binding affinity of -11.95 kcal/mol and an estimated inhibition constant corresponding to 1.73 nM.

We then docked compounds **24** and **28** in the same site, and both wrapped around themselves in the binding pocket (Supplementary Figure S2a,b and S3a,b). Compound **24** optimum pose was predicted with binding affinity of -12.16 kcal/mol and an estimated inhibition constant corresponding to 1.22 nM. Compound **28** was predicted with binding affinity corresponding to -12.34 kcal/mol and an estimated inhibition constant equal to 894.62 pM. Both values were comparable to the estimated free binding energy and the estimated inhibition constant towards (R, S)-ifenprodil, corresponding to -11.95 kcal/mol and to 1.73 nM, respectively.

When both compounds were instead docked to σ1 (PDB 5HK2 [4], Supplementary Figure S4, S5 and S6), Autodock predicted binding affinities and corresponding estimated inhibition constants of compound **24 (**-10.37 kcal/mol and 25.24 nM) as well as those of compound **28** (-10.41 kcal/mol and 23.34 nM) indicated much weaker interactions involved.

We then ran 160 ns of molecular dynamics (MD) simulation on the complexes in water solvent to verify whether the complexes were stable upon simulated time. The ligand topologies were built with ATB [50]. The topologies were validated as the molecular mechanics minimised structure of compound **24** had root mean squared deviation, RMSD, of 0.01009 nm with respect to the semi-empirical minimised structure, while, for compound **28,** the same RMSD was 0.01111 nm.

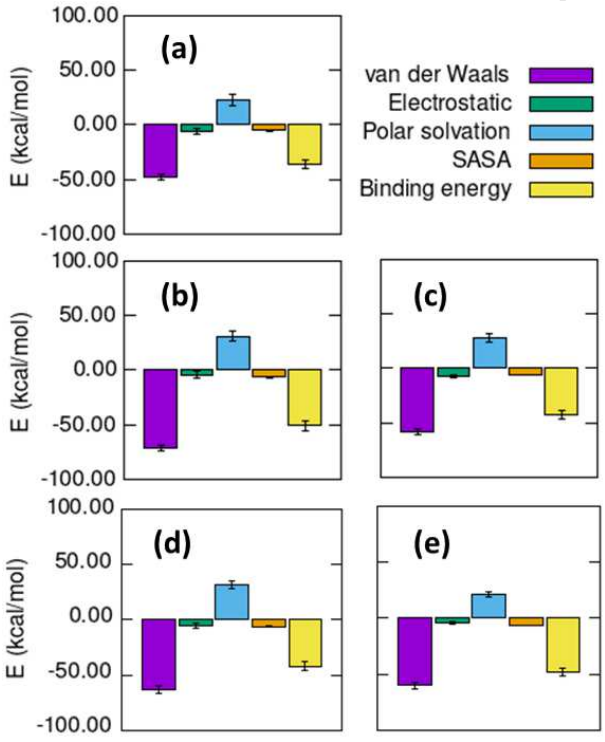

Figure 2. MMPBSA analysis: energetic contributions to the GluN receptor binding of (a) (**R, S)-ifenprodil**, (b) compound **24**, and (c) compound **28** and to the σ1 receptor binding of (d) compound **24**, and (e) compound **28**. Data averaged over the last 60 ns of the molecular dynamic trajectory.

As the simulations were run only on a fragment of the receptor ectodomains, minor rearrangements were expected. Indeed, in all cases the receptor backbone was only slightly rearranged (root mean squared fluctuation, RMSF, not larger than 0.5 nm). While these rearrangements were minor, both compounds explored novel poses (Supplementary Figure S7 and S8). The estimated scores and binding energy values were expected to be not fully comparable with those experimentally determined, we were thus surprised to find that the enthalpic contribution to the binding affinity of both compounds to GluN, in terms of total binding energies (Figure 2), resulted still higher compared to that associated with (R, S)-ifenprodil with an average of 35.7 kcal/mol, while compound **24** was found with an average of 50.9 kcal/mol and **28** with an average of 42.7 kcal/mol. The two appear also tightly bound to σ1: -42.1 kcal/mol for compound **24** and -48.1 kcal/mol for compound **28**.

More thoroughly, both compounds were kept bound to their GluN binding pocket through their neighbouring amino acid and long distance effects were minor (Figure 3a,b). Both compounds interacted with Phe-91 and Tyr-87 from chain A, and in both cases Arg-93 from the same chain opposed the binding due to its strongly unfavourable polar desolvation energy (Figure 3c,d). While in compound **24** also Asp-87 from chain B opposed the binding, Asp-110 from chain A stabilised the molecule through hydrogen bonding with the compound oxygen atoms (Figure 3e,f and Supplementary Figure S9). Along the whole simulation, both molecules remained at the interface between the two chains, as expected (Figure 3e-h).

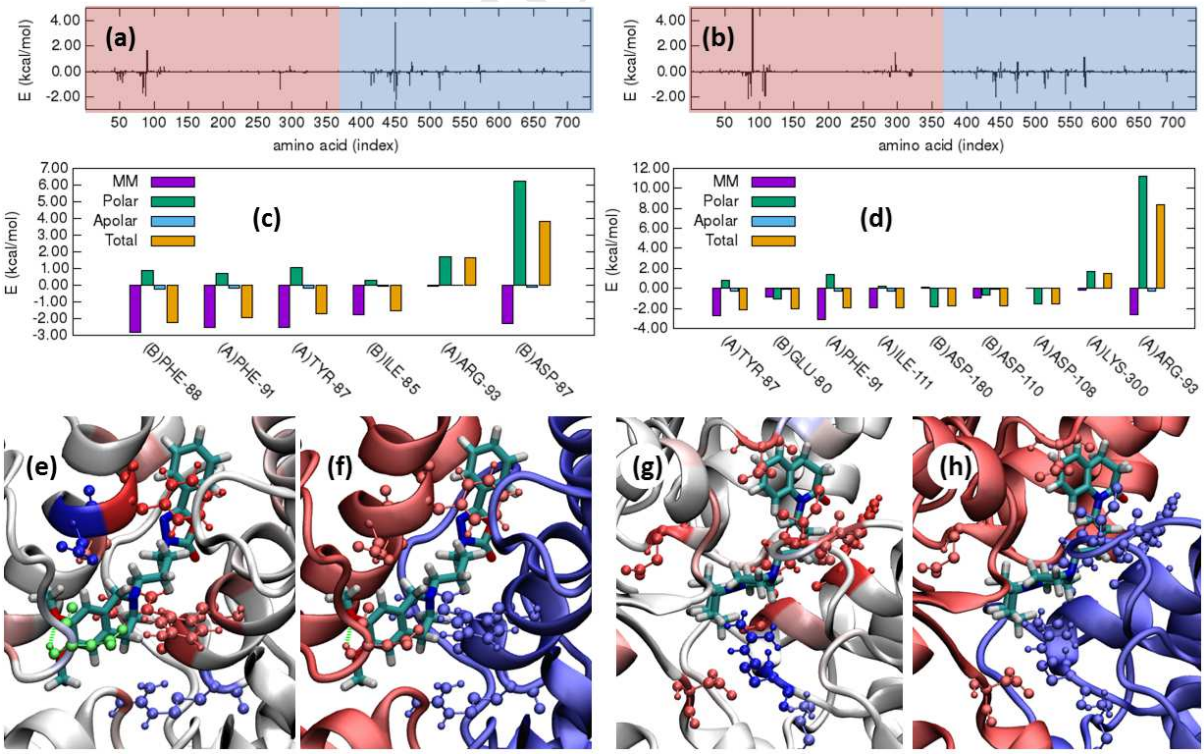

Figure 3. MMPBSA details for GluN bound to compound **24** (left panels) and compound **28** (right panels): (a,b) amino acids contribution to the total binding energy shaded of red/blue highlight chains A/B ; (c,d) details of the contributions of each amino acid with binding energy larger than ± 1.5 kcal/mol; (e-h) close ups on compound **24** and **28** with (e,g) highlighted amino acids with positive (shades of blue) and negative (shades of red) contribution to the binding energy larger than ± 1.5 kcal/mol, hydrogen bonding groups are highlighted in green; (f-h) the same snapshots with GluN1A (chain A, red), GluN2B (chain B, blue).

Rearrangements are also observed for the complex between σ1 and compound **24** (Supplementary Figure S8), but in this case the molecule tends to slip out of its binding site (Figure 4a). Phe-107 and Tyr-120 keep the molecule in place, while Glu-172 and especially Arg-119 strongly opposed to the binding (Figure 4b). The same was not true for compound **28** (Figure 4c), kept in the pocket thanks to Leu-105, Leu-182, and Phe-107 and a hydrogen bond with Thr-181 (Figure 4d, and Supplementary Figure S10).

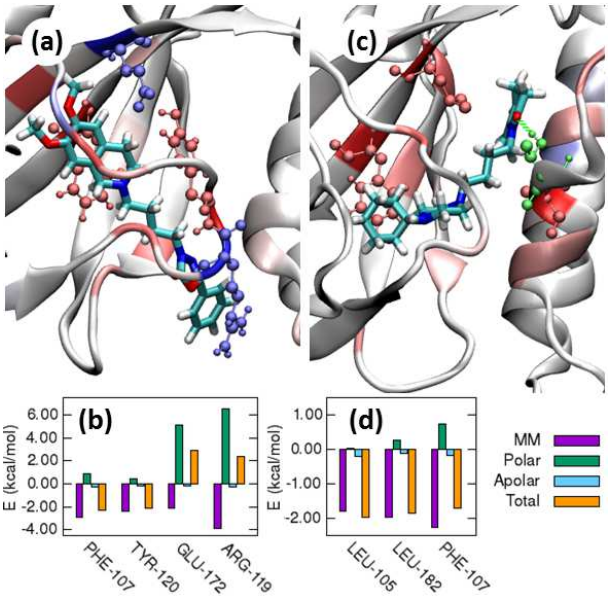

Figure 4. MMPBSA details for sigma1 bound to compound **24** (left panels) and compound **28** (right panels): (a,b) close ups on compound **24** and **28** with highlighted amino acids with positive (shades of blue) and negative (shades of red) contribution to the binding energy larger than ± 1.5 kcal/mol, hydrogen bonding groups are highlighted in green; (c,d) details of the contributions of each amino acid with binding energy larger than ± 1.5 kcal/mol.

Overall, the docking results clearly showed that the binding affinity of the explored compounds towards GluN follows the order **(R, S)-ifenprodil** < **24** < **28**. The trend **24** < **28** was also true towards σ1. Molecular dynamics simulations on the protein fragment corresponding to the binding

domain further confirmed that the molecules were thermodynamically stable in the pinpointed binding site, with the exception of compound **24** tending to slip out of the σ1 pocket.

2.5. Antioxidant activity

2.5.1 Preliminary *in vitro* antioxidant activity evaluation

We further evaluated the antioxidant activity of the most interesting compounds of both phenyloxadiazolone and dihydroquinolinone series (**20, 21, 24, 26-29, 31** and **33**) by testing the ability to scavenge ABTS (2,2'-azino-bis(3-ethylbenzothiazoline-6-sulphonic acid) derived radicals and H_2O_2 (hydrogen peroxide) oxidant . Natural antioxidant ascorbic acid and synthetic antioxidant Trolox (6-hydroxy-2,5,7,8-tetramethylchroman-2-carboxylic acid) were employed as reference standard antioxidants. Most of the compounds potently inhibited ABTS radicals and H_2O_2, compared to the standards (Table 3).

Table 3. Antioxidant activity of compounds **20, 21, 24, 26-29, 31** and **33.**

Cpd	IC_{50} (μg/mL)[a]	
	ABTS	H_2O_2
20	17.96 ± 0.21	21.19 ± 0.52
21	69.25 ± 0.36	73.07 ± 0.65
24	20.95 ± 0.12	27.63 ± 0.39
26	25.47 ± 0.24	31.44 ± 0.48
27	78.80 ± 0.33	84.56 ± 0.55
28	35.79 ± 0.31	38.29 ± 0.61
29	21.34 ± 0.19	24.04 ± 0.45
31	12.35 ± 0.10	15.37 ± 0.41
33	26.24 ± 0.19	29.16 ± 0.28
Ascorbic Acid	13.85 ± 0.19	17.11 ± 0.25
Trolox	22.15 ± 0.22	25.88 ± 0.37

[a]All measurements were performed in triplicate

Compound **31** exhibited a significant radical scavenging capacity on the ABTS with a value of 12.35 ± 0,10, lower than ascorbic acid and Trolox (12.35 vs 13.85 and 12.37 vs 22.15 respectively). Compounds **20, 29** and **31**, showed an important radical scavenging activity on the H_2O_2 (15.37, 24.04 and 21.19). These IC_{50} values were lower than those of the compared standards.

2.5.2 Effects of ligands on H_2O_2-mediated toxicity

The same compounds tested in the aforementioned antioxidant assay were evaluated for cytotoxicity in the human SH-SY5Y (neuroblastoma), HEP3B (hepatocarcinoma) and HeLa (cervical adenocarcinoma) cell lines. As shown in Figure 5, on one hand, the viability of SH-SY5Y cells increased when they were exposed to at low doses (10 µM) of compounds **20**, **26**, **27** and **29**. On the other hand, the lowest cell viability was observed following exposure of all cell lines to compound **20** at 100 µM (Figure 5, Supplementary Table S1). The LD50 values for the selected dual σR/GluN2b selective ligands were calculated from the dose response curves and are shown in Table 4.

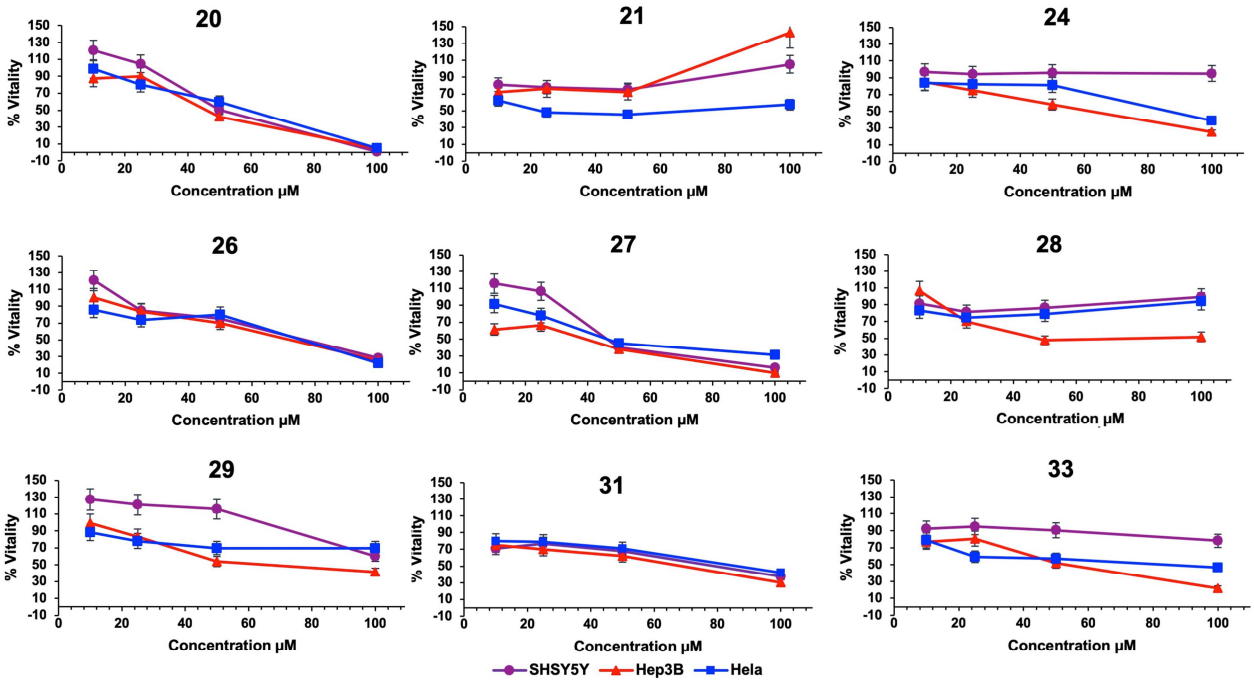

Figure 5. Cell viability of cells treated with the dual σR/GluN2b selective ligands. The cell viability was tested after treatment with the titled compounds **20, 21, 24, 26-29, 31** and **33.** The human neuroblastoma SH-SY5Y (●), human hepatocarcina HEP3B (▲) and human cervical adenocarcinoma HeLa (■) cell lines were treated with increasing concentrations of the dual σR/GluN2b selective ligands for 48h. The cell viability was determined by MTT. The bars represent mean ± SEM of three experiments in triplicate.

Table 4. Cytotoxicity of the dual σR/GluN2b selective ligands to neuroblastoma, hepatocarcinoma and cervical adenocarcinoma cell lines.

Cpd	LD_{50}* (µM)		
	SH-SY5Y	Hep3B	HeLa

20	53 ± 5	51 ± 6	55 ± 5
21	81 ± 7	71 ± 8	76 ± 7
24	77 ± 7	70 ± 5	69 ± 7
26	77 ± 8	70 ± 7	69 ± 8
27	60 ± 5	50 ± 6	55 ± 6
28	493 ± 45	81 ± 9	265 ± 35
29	63 ± 7	77 ± 8	128 ± 15
31	36 ± 5	67 ± 7	83 ± 9
33	231 ± 25	60 ± 7	76 ± 5

*LD_{50} values were calculated from the linear regression of the dose-log response curves after 48 h exposure to the compounds, determined by the MTT assay. Values are mean ± SEM of three experiments in triplicate.

Finally, neuroprotection tests were carried out in the human neuroblastoma SH-SY5Y cell line previously used for studies on the sigma receptors [43, 51] and studies on neuroprotective agents [52, 53]. In order to test the neuroprotective potential of our ligands, H_2O_2 was selected as an appropriate harmful molecule, given that ROS are normally produced in neurons, and, moreover, oxidative stress can be considered the major contributor to cell death in several neurodegenerative disorders [54]. In addition, it has been shown that the loss of cell viability induced by H_2O_2 in the SH-SY5Y cell line is the result of both necrosis and apoptosis [55]. The incubation of SH-SY5Y cells with the σR/GluN2b ligands at the concentration of 25 μM for 48h did not show significant toxicity (Figure 6A). On the other hand, cells exposed to 1000 μM H_2O_2 during 4 h showed a significant of decreased (80%) cellular viability (Figure 6B, DMSO). This observation is consistent with previous studies showing that H_2O_2 induced a loss of SH-SY5Y cells viability [56]. All the tested compounds exhibited a viability > 73% (values ± SEM in Supplementary Tables S2 and S3), after the treatment with H_2O_2. Interestingly, compounds **21** and **28**, both bearing the cyclohexylpiperazine amine moiety, exhibited the best neuroprotective profile, whereas compounds **24** and **31**, both weak σ1R inhibitors, exhibited a slight worsening of cytoprotection. These results, highlight a synergistic effect targeting both σR and GluN2bR, for a neuroprotective action against harmful agents.

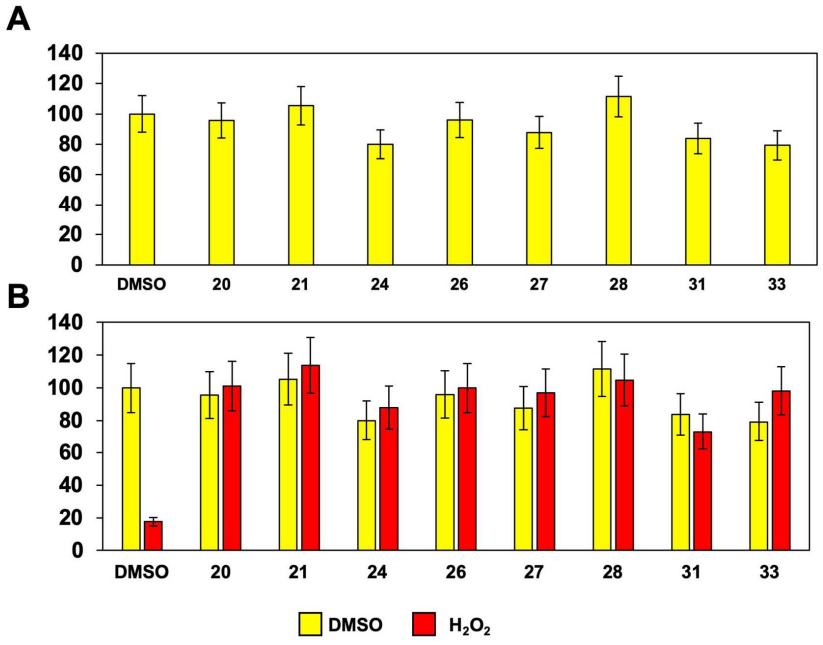

Figure 6. Protective effects of the dual σR/GluN2b selective ligands against H_2O_2 induced neuronal injury. A) Viability of the SH-SY5Y cells treated with 25 μM of the compounds **20, 21, 24, 26-29, 31** and **33**; B) Neuroprotective effects of the selected compounds after treatment of the SH-SY5Y cell line with hydrogen peroxide at 1000 μM. The bars represent the mean ± SEM from three independent experiments performed in triplicate. The differences of all compounds vs DMSO (H_2O_2) were statistically significant, with p value < 0.05.

3. Conclusions

Considering the implication of both σR and GluN2bR in several neurodegenerative disorders, we designed and synthesized two sets of dual receptor modulators endowed with potential neuroprotective properties. Such compounds derived from the combination of different well-known amines moieties with phenyloxadiazolone and dihydroquinolinone scaffolds, previously adopted by us as selective σ1R ligands.

Within the phenyloxadiazolone series, two (**20** and **26**) out of seven compounds showed a pan-affinity towards both σR subtypes but lacked preferential binding. On the other hand, compound **24**

displayed the best selectivity profile for GluN2bR. However, the best results were obtained with the dihydroquinolinones series. Indeed, the cyclohexylpiperazine derivative **28** exhibited the best σR pan-affinity (*K*i σ1 = 21 nM; *K*i σ2 = 1.5 nM) and proved to be 5-fold more powerful (*K*i = 2.0 nM) than the reference drug ifenprodil towards the GluN2b-containing NMDAR subunit. All the compounds possess favourable *in silico* predicted ADME parameters to reach the BBB.

Importantly, most of the compounds were effective in protecting SH-SY5Y cells from H_2O_2-mediated cell death, in particular the cyclohexylpiperazine derivatives **21** and **28**. Therefore, this study suggests that our novel dual σR/GluN2b modulators could be useful as neuroprotective agents that would help to prevent cell death under vulnerability associated with strong ROS production.

From the results obtained, derivatives **24** and **28** could be considered the *hit* compounds to design new selective and more potent σR/GluN2bR ligands.

4. Materials and Methods

4.1 Chemistry, general remarks

Commercially available chemicals were of reagents grade and used as received. Flash chromatography was performed on Silica Gel 60 (70-230 mesh, Sigma-Aldrich-Merck); DCVC (dry-column-vacuum-chromatography) on Silica Gel 40 (230-400 mesh, Sigma-Aldrich-Merck). Reaction courses and product mixtures were routinely monitored by thin-layer chromatography (TLC) on silica gel precoated F_{254} Merck plates. Melting points were determined with a Stuart SMP 300 apparatus and are uncorrected. An Agilent Cary-60 spectrophotometer UV-Vis was employed to record the spectra and quantify the absorbance. Infrared spectra were recorded on a Jasco 4700 spectrophotometer in nujol mulls. Nuclear magnetic resonance spectra were determined on a Varian 400 MHz; ^{1}H-NMR spectra were registered at 400 MHz whereas ^{13}C-NMR were registered at 101 MHz. Chemical shifts are reported as δ (ppm) in $CDCl_3$ solution with the solvent reference relative to tetramethylsilane (TMS) employed as the internal standard ($CDCl_3$, δ = 7.26 ppm for ^{1}H-NMR and δ = 77.2 ppm for ^{13}C-NMR); 1 drop of D_2O was added to assign NH protons. Coupling constants (*J*) are reported in Hz and the splitting abbreviations used are: s, singlet; d, doublet; dd, double doublet; t, triplet; td, triplet of doublets; q, quartet; quint, quintet; m, multiplet; br, broad. Microanalyses (C, H, N) were carried out with Elementar Vario ELIII apparatus and were in agreement with theoretical values ± 0.4%. ESI-MS spectra were obtained on a Bruker Daltonics Esquire 4000 spectrometer by infusion of a solution of the sample in ultrapure MeOH.

4.2 Synthetic procedures

4.2.1 Synthesis of 3-(4-bromobutyl)-5-phenyl-1,3,4-oxadiazol-2(3H)-one **11**

This intermediate was synthesized as previously reported by us [43] starting from benzoic acid hydrazide and triphosgene, to obtain 5-phenyl-1,3,4-oxadiazol-2(3*H*)-one which was converted into 3-(4-bromobutyl)-5-phenyl-1,3,4-oxadiazol-2(3*H*)-one **11** with 1,4-dibromobutane (2.5 eq.), K_2CO_3 (2.5 eq.) as base and a catalytic amount of KI, in ACN at reflux temperature.

White needles solid (upon cooling overnight), yield: 53%; m.p. 64-66 °C; I.R. (nujol, cm^{-1}): 1763; ^{1}H-NMR: ($CDCl_3$/TMS) δ: 1.97 (m, 4H, N-CH_2**CH_2CH_2**CH_2Br), 3.46 (t, 2H, N **CH_2**$CH_2CH_2CH_2$Br, *J* = 8 Hz), 3.83 (t, 2H, N-$CH_2CH_2CH_2$**CH_2**Br, *J* = 8 Hz), 7.48 (m, 3H, arom. Ph), 7.83 (dd, 2H, arom. Ph, *J* = 8 Hz).

4.2.2 Synthesis of 1-(4-bromobutyl)-3,4-dihydrquinolin-2(1H)-one **12**

The procedure for the synthesis of this intermediate is slightly different.

To 0.5 g (3.4 mmol) of the commercially available dihydroquinolin-2(1*H*)-one dissolved in 50 mL of ACN, 1.66 g (5.1 mmol) of $CsCO_3$, 1.1 g (5.1 mmol) of 1.4-dibromobutane and a catalytic amount of TBAB were added. The mixture was allowed to stir at reflux temperature for 14 hours and monitored by TLC (DCM/EtOH 95:5). The solvent was evaporated *in vacuo* and the residue was taken up with DCM and washed with distilled water (3x50). The collected organic phase was dried, filtered and evaporated under reduce pressure to afford a pale-yellow oil.

Yield: 58%; I.R. (nujol, cm^{-1}): 1770; ^{1}H-NMR ($CDCl_3$-TMS) δ: 1.77-1.84 (m, 2H, CH_2**CH_2**CH_2CH_2Br), 1.88-1.95 (m, 2H, CH_2CH_2**CH_2**CH_2Br), 2.63 (t, 2H, CH_2**CH_2**CO dihydroq. *J* = 8 Hz), 2.88 (t, 2H, 2H, **CH_2**CH_2CO dihydroq. *J* = 8 Hz), 3.43 (m, 2H, 2H, $CH_2CH_2CH_2$**CH_2**Br), 3.96 (t, 2H, 2H, **CH_2**$CH_2CH_2CH_2$Br, *J* = 8 Hz), 7.00 (m, 2H, arom.), 7.16-7.24 (m, 2H, arom.).

4.2.3 Amines **13-19**

All amines were purchased from Sigma-Aldrich (Merk) except 7-nitro-1,2,3,4-tetrahydroisoquinoline **18** and 1-(2,4-dimethylphenyl)-*N*-methylmethanamine **19**, the synthesis of which is summarized below.

On an ice bath (0°C), a 100-mL round bottom flask with 1.3 g (10 mmol) of 1,2,3,4-tetrahydroquinoline and 5 mL of conc. H_2SO_4 was allowed to stir for 10 minutes. To this solution, 1.1 g (10 mmol) of KNO_3 were added in small portions, taking care that the temperature of the reaction did not rise above 5°C. The reaction was stirred overnight and monitored by TLC

(DCM/EtOH 90:10). The brown solution was neutralized with a solution of diluted NH_4OH until pH = 8 and the basic mixture was extracted with DCM (3x50 mL). The combined organic extracts were washed with brine (once), dried and filtered. The evaporation of the solvent affords a red oil which was dissolved in the minimum amount of abs. EtOH and cooled on an ice bath. The alcoholic solution was treated with 2.5 mL of conc. HCl to affords a yellow precipitate of 7-nitro-1,2,3,4-tetrahydroisoquinoline **18**, which was recrystallized from MeOH.

Yellow solid; m.p.: 261-263 (260-262°C [57]); Yield: 32%; I.R. (nujol, cm^{-1}): 3173; ^{1}H-NMR ($CDCl_3$-TMS) δ: 1.86 (br s, 1H, NH disapp. on D_2O), 3.12 (t, 2H, H-4, *J* = 8 Hz), 3.46 (t, 2H, H-3, *J* = 8 Hz), 4.37 (s, 2H, H-1), 7.36 (d, 1H, arom. H-5, *J* = 12 Hz), 8.00 (m, 2H, arom. H-6 and H-8).

The synthesis of **19** started from 2,4-dimethylbenzaldheyde (5 g, 37.3 mmol) which was dissolved in 20 mL of abs. EtOH and then added of 2.32 g of methylamine solution (33% in EtOH, 74.6 mmol). The mixture was allowed to heated at 40°C for 1 hours (monitored by TLC) then cooled, the solvent and the excess of methylamine were eliminated under reduced pressure. The residual solid of (Z/E)-N-(2,4-dimethylbenzylidene)methanamine (5.45 g, 37.0 mmol), was treated with a slight excess of $NaBH_4$ (2.1 g, 55.6 mmol) in abs. EtOH at 0°C; the mixture was stirred at room temperature overnight. The resulting mixture was evaporated *in vacuo*, poured into distilled water and extracted with DCM (3x150 mL). The collected organic phase was dried, filtered and finally evaporated to affords 5.4 g of **19** as a light-yellow semisolid (upon cooling).

Yield: 98%; I.R. (nujol, cm^{-1}): 3166; ^{1}H-NMR ($CDCl_3$-TMS) δ: 1.52 (br, 1H, NH disapp. on D_2O), 2.31 (s, 3H, CH_3 arom.), 2.33 (s, 3H, CH_3 arom.), 2.50 (s, 3H, NCH_3), 3.71 (s, 2H, CH_2), 7.00 (m, 2H, arom.), 7.17 (d, 1H, arom. *J* = 8 Hz).

4.2.4 General synthesis of the final compounds **20-33**

To a solution of 0.2 g (0.67 mmol) of **11**, 0.19 g (1.35 mmol) of K_2CO_3, a catalytic amount of KI and 3*H*-spiro[isobenzofuran-1,4'-piperidine] hydrochloride **13** (0.15 g, 0.67 mmol) in ACN (30 mL) was heated at reflux temperature for 24 h and monitored by TLC until the reaction was completed. The hot solution was filtered and concentrated *in vacuo* to give 0.3 g of **20**.

4.2.4.1 3-(4-(3H-spiro[isobenzofuran-1,4'-piperidin]-1'-yl)butyl)-5-phenyl-1,3,4-oxadiazol-2(3H)-one **20**

Light-red oil; Yield: 92%; I.R. (nujol, cm^{-1}): 1775; ^{1}H-NMR ($CDCl_3$-TMS) δ: 1.58-2.00 (m, 8H, CH_2**CH_2CH_2**CH_2 and 2xCH_2 pip.), 2.38 (td, 2H, pip. *J* = 2.4 and 12.0 Hz), 2.46 (t, 2H,

CH$_2$CH$_2$CH$_2$CH$_2$, *J* = 7.6 Hz), 2.84 (br d, 2H, pip. *J* = 10.4 Hz), 3.83 (t, 2H, CH$_2$CH$_2$CH$_2$**CH$_2$**, *J* = 7.2 Hz), 5.05 (s, 2H, OCH$_2$ fur.), 7.10-7.27 (m, 4H, arom. isobenzofuran), 7.47 (m, 3H, arom. phenyl), 7.83 (m, 2H, arom. phenyl). ^{13}C-NMR (CDCl$_3$-TMS) δ: 24.0, 26.3, 36.6, 45.9, 50.2, 58.2, 70.7, 84.7, 120.8, 121.0, 123.9, 125.6, 127.3, 127.5, 128.9, 131.5, 138.9, 145.65, 153.2, 153.6. MS: *m/z* 406 [MH$^+$]. Anal. calcd for C$_{24}$H$_{27}$N$_3$O$_3$ (%): C, 71.09; H, 6.71; N, 10.36. Found: C, 71.11; H, 6.74; N, 10.18.

Following the same procedure described above (only 1 equivalent of K$_2$CO$_3$ when amines are as free-bases), compounds **21-33** were synthesized.

4.2.4.2 3-(4-(4-Cyclohexylpiperazin-1-yl)butyl)-5-phenyl-1,3,4-oxadiazol-2(3H)-one **21**.

Pale-yellow Oil; Yield: 94%; I.R. (nujol, cm^{-1}): 1778; ^{1}H-NMR (CDCl$_3$-TMS) δ: 1.03-126 (m, 5H, (C**H**H)$_5$) cyclohex.), 1.56-1.86 (m, 9H, CH$_2$**CH$_2$CH$_2$**CH$_2$ and (CH**H**)$_5$) cyclohex.), 2.18 (m, 1H, CH cyclohex.), 2.35 (t, 2H, CH$_2$CH$_2$CH$_2$**CH$_2$**, *J* =7.6 Hz), 2.45 (br m, 4H, pip.), 2.56 (br m, 4H pip.), 3.78 (t, 2H, **CH$_2$**CH$_2$CH$_2$CH$_2$ *J* = 7.2 Hz), 7.45 (m, 3H, arom. phenyl), 7.80 (m, 2H, arom. phenyl). ^{13}C-NMR (CDCl$_3$-TMS) δ: 23.7, 25.9, 26.2, 26.3, 28.9, 45.8, 48.9, 53.7, 57.9, 63.4, 123.9, 125.6, 128.9, 131.4, 153.1, 153.6. MS: *m/z* 385 [MH$^+$]. Anal. calcd for C$_{22}$H$_{32}$N$_4$O$_2$ (%): C, 68.72; H, 8.39; N, 14.57. Found: C, 68.76; H, 8.40; N, 14.58.

4.2.4.3 3-(4-(4-(4-Fluorophenyl)piperazin-1-yl)butyl)-5-phenyl-1,3,4-oxadiazol-2(3H)-one **22**.

Pale-brown oil (purified after trituration with petroleum ether); Yield: 69%; I.R. (nujol, cm^{-1}): 1782; ^{1}H-NMR (CDCl$_3$-TMS) δ: 1.63 (quint, 2H, CH$_2$CH$_2$**CH$_2$**CH$_2$, *J* = 7.2 Hz), 1.87 (quint, 2H, CH$_2$**CH$_2$**CH$_2$CH$_2$, *J* = 7.2 Hz), 2.44 (t, 2H, CH$_2$CH$_2$CH$_2$**CH$_2$**, *J* = 7.6 Hz), 2.59 (t, 4H, pip. *J* = 4.8 Hz), 3.10 (t, 4H, pip. *J* = 4.8 Hz), 3.83 (t, 2H, **CH$_2$**CH$_2$CH$_2$CH$_2$, *J* = 7.6 Hz), 6.86 (m, 2H, arom. *p*-F-phenyl), 6.94 (m, 2H, arom. *p*-F-phenyl), 7.47 (m, 3H, arom. phenyl), 7.83 (m, 2H, arom. phenyl). ^{13}C-NMR (CDCl$_3$-TMS) δ: 23.7, 26.2, 45.8, 50.1, 53.2, 57.7, 115.3 (2), 115.6 (2), 117.7, 117.8, 117.9, 123.9, 125.6, 128.9, 131.5, 147.9, 148.0, 153.2, 153.6, 155.9, 158.3. MS: *m/z* 397 [MH$^+$]. Anal. calcd for C$_{22}$H$_{25}$FN$_4$O$_2$ (%): C, 66.65; H, 6.36; N, 14.13. Found: C, 66.69; H, 6.34; N, 14.11.

4.2.4.4 5-Phenyl-3-(4-(4-(pyridin-2-yl)piperazin-1-yl)butyl)-1,3,4-oxadiazol-2(3H)-one **23**.

Yellow Oil; Yield: 96%; I.R. (nujol, cm^{-1}): 1776; ^{1}H-NMR (CDCl$_3$-TMS) δ: 1.59 (quint, 2H, CH$_2$CH$_2$**CH$_2$**CH$_2$, *J* = 7.2 Hz), 1.85 (quint, 2H, CH$_2$**CH$_2$**CH$_2$CH$_2$, *J* = 7.2 Hz), 2.41 (td, 2H, CH$_2$CH$_2$CH$_2$**CH$_2$**, *J* = 1.2 and 7.2 Hz), 2.51 (t, 4H, pip. *J* = 4.8 Hz), 3.51 (t, 4H, pip. *J* = 4.8 Hz),

3.81 (t, 2H, **CH$_2$**CH$_2$CH$_2$CH$_2$, *J* = 1.2 and 7.2 Hz), 6.59 (m, 2H, arom. pyr.), 7.80 (d, 2H, arom. phenyl, *J* = 8.0 Hz), 8.15 (m, 2H, arom. phenyl). ^{13}C-NMR (CDCl$_3$-TMS) δ: 23.7, 26.2, 45.2, 45.8, 53.0, 57.8,107.0, 113.2, 123.9, 125.6, 128.9, 131.5, 137.4, 147.9, 153.1, 153.6, 159.5. MS: *m/z* 380 [MH$^+$]. Anal. calcd for $C_{21}H_{25}N_5O_2$ (%): C, 66.47; H, 6.64; N, 18.46. Found: C, 66.50; H, 6.44; N, 18.55.

4.2.4.5 3-(4-(6,7-Dimethoxy-3,4-dihydroisoquinolin-2(1H)-yl)butyl)-5-phenyl-1,3,4-oxadiazol-2(3H)-one **24**.

Brown oil (purified by dry-flash chromatography with DCM as eluant); Yield: 57%; I.R. (nujol, cm^{-1}): 1767; ^{1}H-NMR (CDCl$_3$-TMS) δ: 1.66 (quint, 2H, CH$_2$CH$_2$**CH$_2$**CH$_2$, *J* = 7.2 Hz), 1.89 (quint, 2H, CH$_2$**CH$_2$**CH$_2$CH$_2$, *J* = 7.2 Hz), 2.54 (t, 2H, CH$_2$CH$_2$CH$_2$**CH$_2$**, *J* = 7.2 Hz), 2.68 (t, 2H, H-4, dihydroisoquin. *J* = 5.6 Hz), 2.79 (t, 2H, H-3, dihydroisoquin. *J* = 5.6 Hz), 3.52 (s, 2H, H-9, dihydroisoquin.), 3.81 (m, 8H, 2x OCH$_3$ and **CH$_2$**CH$_2$CH$_2$CH$_2$), 6.49 (s, 1H, H-5, arom. dihydroisoquin.), 6.56 (s, 1H, H-8, arom. dihydroisoquin.), 7.45 (m, 3H, arom. phenyl), 7.81 (m, 2H, arom. phenyl). ^{13}C-NMR (CDCl$_3$-TMS) δ: 24.0, 26.2, 28.7, 45.8, 51.0, 55.7, 55.9, 57.4, 109.1, 111.3, 123.9, 125.6 (2), 126.2, 126.5 (2), 128.9 (2), 131.4, 131.5, 147.1, 147.4, 153.1, 153.6. MS: *m/z* 410 [MH$^+$]. Anal. calcd for $C_{23}H_{27}N_3O_4$ (%): C, 67.46; H, 6.65; N, 10.26. Found: C, 67.50; H, 6.67; N, 10.29.

4.2.4.6 3-(4-(7-Nitro-3,4-dihydroisoquinolin-2(1H)-yl)butyl)-5-phenyl-1,3,4-oxadiazol-2(3H)-one **25**.

Brown oil; Yield: 99%; I.R. (nujol, cm^{-1}): 1777; ^{1}H-NMR (CDCl$_3$-TMS) δ: 1.68 (quint, 2H, CH$_2$CH$_2$**CH$_2$**CH$_2$, *J* = 7.2 Hz), 1.91 (quint, 2H, CH$_2$**CH$_2$**CH$_2$CH$_2$, *J* = 7.2 Hz), 2.59 (t, 2H, CH$_2$CH$_2$CH$_2$**CH$_2$**, *J* = 7.2 Hz), 2.75 (t, 2H, H-4, dihydroisoquin. *J* = 5.6 Hz), 2.97 (t, 2H, H-3, dihydroisoquin. *J* = 5.6 Hz), 3.67 (s, 2H, H-9, dihydroisoquin.), 3.85 (t, 2H, **CH$_2$**CH$_2$CH$_2$CH$_2$, *J* = 7.6 Hz), 7.22 (d, 1H, H-5, arom. dihydroisoquin. *J* = 8.4 Hz), 7.46 (m, 3H, H-8, arom. phenyl), 7.81 (m, 2H, arom. phenyl), 7.88 (d, 1H, H-8 arom. dihydroisoquin. *J* = 2.4 Hz), 7.95 (dd, 1H, arom. phenyl, *J* = 2.4 and 8.4 Hz). ^{13}C-NMR (CDCl$_3$-TMS) δ: 23.8, 26.0, 29.4, 45.7, 50.1, 55.7, 57.2, 121.1, 121.7, 123.8, 125.6, 128.9, 129.5, 131.5, 136.4, 142.4, 153.2, 153.6. MS: *m/z* 395 [MH$^+$]. Anal. calcd for $C_{21}H_{22}N_4O_4$ (%): C, 63.95; H, 5.62; N, 14.20. Found: C, 63.97; H, 5.64; N, 14.24.

4.2.4.7 3-(4-((2,4-Dimethylbenzyl)(methyl)amino)butyl)-5-phenyl-1,3,4-oxadiazol-2(3H)-one **26**.

Pale-yellow oil; Yield: 98%; I.R. (nujol, cm^{-1}): 1760; ^{1}H-NMR ($CDCl_3$-TMS) δ: 1.58 (m, 2H, $CH_2CH_2\mathbf{CH_2}CH_2$), 1.84 (m, 2H, $CH_2\mathbf{CH_2}CH_2CH_2$), 2.15 (s, 3H, NCH_3), 2.29 (s, 3H, CH_3 arom.), 2.32 (s, 3H, CH_3 arom.), 2.42 (t, 2H, $CH_2CH_2CH_2\mathbf{CH_2}$, *J* = 8 Hz), 3.39 (s, 2H, CH_2-Ph), 3.78 (t, 2H, $\mathbf{CH_2}CH_2CH_2CH_2$, *J* = 8 Hz), 6.95 (m, 2H, arom.), 7.13 (d, 1H, arom. *J* = 8 Hz), 7.46 (m, 3H, arom), 7.84 (dd, 2H, arom. phenyl, *J* = 4 and 8 Hz). ^{13}C-NMR ($CDCl_3$-TMS) δ: 19.1, 21.0, 24.3, 26.0, 41.9, 45.9, 56.8, 60.4, 76.7, 77.4, 124.0, 125.6 (2), 126.1, 128.9, 129.0, 129.8, 131.0, 131.4, 134.2, 136.4, 137.1, 153.1, 153.6. MS: *m/z* 366 [MH^+]. Anal. calcd for $C_{22}H_{27}N_3O_2$ (%): C, 72.30; H, 7.45; N, 11.50. Found: C, 72.33; H, 7.45; N, 11.47.

4.2.4.8 1-(4-(3H-spiro[isobenzofuran-1,4'-piperidin]-1'-yl)butyl)-3,4-dihydroquinolin-2(1H)-one **27**.

Pale-brown oil; Yield: 95%; I.R. (nujol, cm^{-1}): 1687; ^{1}H-NMR ($CDCl_3$-TMS) δ: 1.60-1.85 (m, 6H, $CH_2\mathbf{CH_2CH_2}CH_2$ and CH_2 pip.), 2.00 (m, 2H, CH_2 pip.), 2.38 (br td, 2H, pip. *J* = 4 and 12 Hz), 2.46 (t, 2H, $\mathbf{CH_2}CH_2CH_2CH_2$ *J* = 7.2 Hz), 2.61 (m, 2H, CH_2 (C$\mathbf{HH_{3,3'}}$) dihydroquin.), 2.86 (m, 3H, (C$\mathbf{HH_{4,4'}}$) dihydroquin. and pip.), 3.15 (br td, 1H, pip. *J* = 2.4 and 8.8 Hz), 3.96 (t, 2H, $CH_2CH_2CH_2\mathbf{CH_2}$, *J* = 7.2 Hz), 5.05 (s, 2H, OCH_2 fur.), 6.95-7.27 (m, 8H, arom.). ^{13}C-NMR ($CDCl_3$-TMS) δ: 24.2, 25.1, 25.6, 31.9, 36.6, 41.9, 50.1, 58.2, 70.7, 84.7, 114.9, 120.8, 121.0, 122.7, 126.6, 127.3, 127.4, 127.5, 128.0, 138.9, 145.6, 170.1. MS: *m/z* 391 [MH^+]. Anal. calcd for $C_{25}H_{30}N_2O_2$ (%): C, 76.89; H, 7.74; N, 7.17. Found: C, 76.93; H, 7.55; N, 7.47.

4.2.4.9 1-(4-(4-Cyclohexylpiperazin-1-yl)butyl)-3,4-dihydroquinolin-2(1H)-one **28**.

Reddish oil (purified by column chromatography using DCM/EtOH 95-5 then DCM/EtOH 90-10 as eluant); Yield: 56%; I.R. (nujol, cm^{-1}): 1670; ^{1}H-NMR ($CDCl_3$-TMS) δ: 1.19 (m, 5H, (C**H**H)$_5$ cyclohex.), 1.55-1.83 (m, 6H, $CH_2\mathbf{CH_2CH_2}CH_2$ and (CH**H**)$_5$ cyclohex.), 2.24 (m, 1H, N-CH cyclohex.), 2.35 (t, 2H, $CH_2CH_2CH_2\mathbf{CH_2}$, *J* = 7.2 Hz), 2.48 (br m, 4H, pip.), 2.59 (m, 6H, pip., cyclohex. and (C$\mathbf{HH_{3,3'}}$) dihydroquin.), 2.85 (t, 2H, (C$\mathbf{HH_{4,4'}}$) dihydroquin. *J* = 7.2 and 8.0 Hz), 3.91 (t, 2H, $\mathbf{CH_2}CH_2CH_2CH_2$ *J* = 7.2 and 8.0 Hz), 6.96 (td, 1H, H-6 arom. dihydroquin. *J* = 1.2 and 7.2 Hz), 7.02 (d, 2H, H-5 arom. dihydroquin. *J* = 8.0 Hz), 7.12 (br d, 2H, H-8 arom. dihydroquin. *J* = 7.6 Hz), 7.20 (td, 2H, H-7 arom. dihydroquin. *J* = 1.6 and 8.4 Hz). ^{13}C-NMR ($CDCl_3$-TMS) δ: 23.9, 24.9, 25.6, 25.8, 26.2, 28.8, 31.9, 41.8, 48.8, 53.3, 53.4, 57.8, 63.6, 114.9, 122.6, 126.5, 127.3, 127.9, 139.5, 170.0. MS: *m/z* 370 [MH^+]. Anal. calcd for $C_{23}H_{35}N_3O$ (%): C, 74.75; H, 9.55; N, 11.37. Found: C, 74.73; H, 9.55; N, 11.36.

4.2.4.10 1-(4-(4-(4-fluorophenyl)piperazin-1-yl)butyl)-3,4-dihydroquinolin-2(1H)-one **29**.

Pale-yellow oil (purified column chromatography using DCM 100 then DCM/EtOH 94-6 as eluant); Yield: 35%; I.R. (nujol, cm^{-1}): 1675; ^{1}H-NMR ($CDCl_3$-TMS) δ: 1.61 (quint, 2H, $CH_2CH_2\mathbf{CH_2}CH_2$, *J* = 7.2), 1.71 (m, 2H, $CH_2\mathbf{CH_2}CH_2CH_2$ *J* = 7.2), 2.44 (t, 2H, $CH_2CH_2CH_2\mathbf{CH_2}$, *J* = 7.6 Hz), 2.60 (t, 4H, pip. *J* = 5.2 Hz), 2.64 (m, 2H, (C**HH$_{3,3'}$**) dihydroquin.), 2.88 (td, 2H, pip. *J* = 6.8 Hz), 3.12 (t, 2H, (C**HH$_{4,4'}$**) dihydroquin. *J* = 5.2 Hz), 3.97 (t, 2H, $\mathbf{CH_2}CH_2CH_2CH_2$, *J* = 7.2 Hz), 6.88 (m, 2H, arom. *p*-F-phenyl), 6.94 (m, 2H, arom. *p*-F-phenyl), 6.99 (m, 1H, H-6 arom. dihydroquin.), 7.06 (dd, 1H, H-5 arom. dihydroquin., *J* = 1.2 and 7.6 Hz), 7.16 (dd, 1H, H-8 arom. dihydroquin., *J* = 1.2 and 7.6 Hz), 7.23 (td, 1H, H-7 arom. dihydroquin., *J* = 1.6 and 7.6 Hz). ^{13}C-NMR ($CDCl_3$-TMS) δ: 24.0, 24.9, 25.6, 31.9, 41.8, 50.1, 57.8, 114.9, 115.3, 117.7, 117.8, 122.7, 127.4, 127.8, 139.5, 148.0 (2), 155.9, 158.3, 170.1. MS: *m/z* 382 [MH^+]. Anal. calcd for $C_{23}H_{28}FN_3O$ (%): C, 72.41; H, 7.40; N, 11.01. Found: C, 72.43; H, 7.40; N, 11.03.

4.2.4.11 1-(4-(4-(pyridine-2-yl)piperazin-1-yl)butyl)-3,4-dihydroquinolin-2(1H)-one **30**.

Pale-yellow oil (purified by column chromatography using DCM 100 then DCM/EtOH 95-5 as eluant); Light-yellow Oil; Yield: 36%; I.R. (nujol, cm^{-1}): 1685; ^{1}H-NMR ($CDCl_3$-TMS) δ: 1.58-1.75 (m, 4H, $CH_2\mathbf{CH_2CH_2}CH_2$), 2.43 (t, 2H, $CH_2CH_2CH_2\mathbf{CH_2}$, *J* = 7.2 Hz), 2.51 (t, 4H, pip. *J* = 4.8 Hz), 2.63 (m, 2H, (C**HH$_{3,3'}$**) dihydroquin.), 2.89 (td, 2H, (C**HH$_{4,4'}$**) dihydroquin. *J* = 6.8 Hz), 3.54 (t, 4H, pip. *J* = 5.2 Hz), 3.97 (t, 2H, $\mathbf{CH_2}CH_2CH_2CH_2$, *J* = 7.2 Hz), 6.63 (m, 2H, arom. pyr.), 6.99 (td, 1H, arom. *J* = 1.2 and 7.2 Hz), 7.06 (d, 1H, arom. *J* = 8.4 Hz), 7.16 (dd, 1H, arom. *J* = 1.6 and 7.6 Hz), 7.23 (td, 1H, arom. pyr. *J* = 1.6 and 7.6 Hz), 7.47 (m, 1H, arom. pyr.), 8.18 (m, 1H, arom. pyr.). ^{13}C-NMR ($CDCl_3$-TMS) δ: 23.9, 24.9, 25.5, 31.9, 41.8, 45.2, 53.0, 57.9, 107.0, 113.2, 114.9, 122.6, 126.5, 127.4, 128.0, 137.4, 139.5, 147.9, 159.5, 170.1. MS: *m/z* 365 [MH^+]. Anal. calcd for $C_{22}H_{28}N_4O$ (%): C, 72.50; H, 7.74; N, 15.37. Found: C, 72.53; H, 7.54; N, 15.37.

4.2.4.12 1-(4-(6,7-dimethoxy-3,4-dihydroisoquinolin-2(1H)-yl)butyl)-3,4-dihydroquinolin-2(1H)-one **31**.

Reddish oil (purified by dry-flash chromatography with DCM then DCM/EtOH 94-6 as eluant); Yield: 65%; I.R. (nujol, cm^{-1}): 1660; ^{1}H-NMR ($CDCl_3$-TMS) δ: 1.68 (quint, 2H, $CH_2CH_2\mathbf{CH_2}CH_2$, *J* = 7.2), 1.78 (quint, 2H, $CH_2\mathbf{CH_2}CH_2CH_2$, *J* = 7.2), 2.56 (m, 2H, $CH_2CH_2CH_2\mathbf{CH_2}$), 2.81 (m, 4H, (C**HH$_{4,4'}$**) dihydroisoquin. and (C**HH$_{3,3'}$**) dihydroquin.), 2.94 (m, 4H, (C**HH$_{3,3'}$**) dihydroisoquin. and (C**HH$_{4,4'}$**) dihydroquin.), 3.77 (ds, 6H, 2x OCH_3), 3.81 (s, 2H, (C**HH$_{9,9'}$**) dihydroisoquin.), 3.91 (t, 2H, $\mathbf{CH_2}CH_2CH_2CH_2$, *J* = 7.2 Hz), 6.48 (s, 1H, H-5, arom. dihydroisoquin.), 6.54 (s, 1H, H-8,

arom. dihydroisoquin.), 6.91 (td, 1H, H-6, arom. dihydroquin. *J* = 1.2 and 7.2 Hz), 6.97 (td, 1H, H-5, arom. dihydroquin. *J* = 1.2 and 7.2 Hz), 7.09 (t, 1H, H-5, arom. dihydroquin. *J* = 8 Hz). ^{13}C-NMR ($CDCl_3$-TMS) δ: 22.0, 23.7, 24.5, 25.5, 30.9, 40.3, 49.1, 53.2, 54.9, 55.0, 55.1, 108.4, 110.2, 113.9, 121.8, 123.5, 125.5, 126.5, 127.0, 138.2, 146.7, 147.2, 169.3. MS: *m/z* 395 [MH^+]. Anal. calcd for $C_{24}H_{30}N_2O_3$ (%): C, 73.07; H, 7.10; N, 15.37. Found: C, 73.11; H, 7.14; N, 15.39.

4.2.4.13 1-(4-(7-nitro-3,4-dihydroisoquinolin-2(1H)-yl)butyl)-3,4-dihydroquinolin-2(1H)-one **32**.
Brownish oil (purified by dry-flash chromatography with DCM then DCM/EtOH 98-2 as eluant); Yield: 30%; I.R. (nujol, cm^{-1}): 1674; ^{1}H-NMR ($CDCl_3$-TMS) δ: 1.70 (m,4H, CH_2**CH_2**CH_2**CH_2**CH_2), 2.60 (m, 4H, $CH_2CH_2CH_2$**CH_2** and (C**$HH_{4,4'}$**) dihydroisoquin.), 2.75 (t, 2H, (C**$HH_{3,3'}$**) dihydroquin. *J* = 6.0 Hz), 2.87 (m, 2H, (C**$HH_{4,4'}$**) dihydroquin), 2.97 (t, 2H, (C**$HH_{3,3'}$**) dihydroisoquin. *J* = 6.0 Hz), 3.67 (s, 2H, H-9, dihydroisoquin.), 3.98 (t, 2H, **CH_2**$CH_2CH_2CH_2$, *J* = 7.2 Hz), 6.97 (td, 1H, H-6, arom. dihydroquin. *J* = 1.2 and 7.2 Hz), 7.04 (d, 1H, H-5, arom. dihydroisoquin. *J* = 7.6 Hz), 7.13 (m, 2H, H-5,8, arom. dihydroquin.), 7.23 (d, 2H, H-7, arom. dihydroquin. *J* = 7.6 Hz), 7.90 (d, 1H, H-8 dihydroisoq. *J* = 2.4 Hz), 7.96 (dd, 1H, H-6 dihydroisoq. *J* = 2.4 and 7.6 Hz). ^{13}C-NMR ($CDCl_3$-TMS) δ: 24.1, 24.8, 25.6, 29.4, 31.9, 41.7, 50.0, 55.7, 57.2, 114.8, 121.1, 121.8, 122.7, 126.6, 127.3, 128.0, 129.5, 136.4, 139.4, 142.5, 146.0, 170.1. MS: *m/z* 380 [MH^+]. Anal. calcd for $C_{22}H_{25}N_3O_3$ (%): C, 69.64; H, 6.64; N, 11.07. Found: C, 69.63; H, 6.62; N, 11.07.

4.2.4.14 1-(4-((2,4-dimethylbenzyl)(methyl)amino)butyl)-3,4-dihydroquinolin-2(1H)-one **33**.
Pale-red oil; Yield: 96%; I.R. (nujol, cm^{-1}): 1689; ^{1}H-NMR ($CDCl_3$-TMS) δ: 1.58 (quint, 2H, CH_2CH_2**CH_2**CH_2, *J* = 7.2 Hz), 1.67 (quint, 2H, CH_2**CH_2**CH_2CH_2, *J* = 7.2 Hz), 2.14 (s, 3H, NCH_3), 2.29 (s, 3H, CH_3 arom.), 2.30 (s, 3H, CH_3 arom.), 2.41 (t, 2H, $CH_2CH_2CH_2$**CH_2**, *J* = 7.2 Hz), 2.63 (m, (C**$HH_{3,3'}$**) dihydroquin.), 2.88 (m, (C**$HH_{4,4'}$**) dihydroquin.), 3.38 (s, 2H, CH_2-Ph), 3.93 (t, 2H, **CH_2**$CH_2CH_2CH_2$, *J* = 7.6 Hz), 6.97 (m, 4H, arom.), 7.14 (m, 1H, arom.), 7.23 (td, 1H, arom. *J* = 2.4 and 7.6 Hz). ^{13}C-NMR ($CDCl_3$-TMS) δ: 19.2, 21.0, 24.8, 25.1, 25.6, 31.9, 42.0, 42.1, 57.4, 60.1, 114.9 (2), 122.6, 126.1, 126.6, 127.4, 127.9, 128.0, 129.8, 131.0, 134.2, 136.3, 137.1, 139.6, 170.1. MS: *m/z* 351 [MH^+]. Anal. calcd for $C_{23}H_{30}N_2O$ (%): C, 78.82; H, 8.63; N, 7.99. Found: C, 78.85; H, 8.66; N, 7.87.

4.3 Computational studies

4.3.1 Docking

We chose for GluN chains A and B from structure 4PE5 [41] as template, while for σ1 we chose chain C from structure 5HK2 [4]. We reconstructed the missing atoms and residues with Swiss-Model [58]. Molecules initial conformation were minimized with AM1 method as implemented in MOPAC [59]. Each system to be docked was then prepared with AutoDock tools, and docked with AutoDock [60]. We used Lamarckian Genetic Algorithm with docking box centered on the ligand and 70x40x30 grid points for GlunN, and docking box centered on Tyr 103 hydroxylic oxygen and 40x42x40 grid points for σ1, in both cases with spacing 0.375Å. The docking was performed with 10 runs and 25,000,000 maximum numbers of evaluations and standard parameters. 2D ligand-protein interaction diagrams were generated with LigPlot+[61].

4.3.2 Molecular Dynamics Simulations

We consider complexes formed by the ligands with the first 370 amino acids of both chain A and chain B for GluN, and with residues between 40 and 210 for σ1. We minimized each complex by first minimizing the protein side chains alone, then whole protein and finally the whole system by constraining selected portions of the system. We placed each complex in a cubic box with a water layer of 0.7 nm and performed a second minimization. We used GROMOS force field and Simple Point Charge water. Ligand topologies were built with ATB [50]. We performed NVP and NPT equilibrations for 100 ps, followed by 160 ns NPT production run at 300 K. The iteration time step was set to 2 fs with the Verlet integrator and LINCS [62] constraint. We used periodic boundary conditions. All the simulations and their analysis were run as implemented in the Gromacs package v. 2016.1 [63]. RMSDs and RMSF have been calculated from configurations sampled every 10ps and as running averages over 100 sampled points. VINA scorings were calculated over configurations sampled every 100 ps and as running averages over 10 points. 2D ligand-protein interaction diagrams were generated with LigPlot+ [61]. The binding free energy was estimated with the MM/PBSA method, with the apolar solvation energy calculated as solvent accessible surface area (SASA) and default parameters, as implemented in the g_mmpbsa tool [64]. Simulations were run on Marconi (CINECA, Italy).

4.4 Physiochemical and Pharmacokinetics parameters

The physiochemical and pharmacokinetics parameter of compounds **20**-**33** was calculated using Marvinsketch® (Chemaxon) software and the BBB scores were predicted with algorithm of central nervous system multiparameter optimization (CNS MPO) developed by Wager *et al.* [48].

4.5 Binding studies

4.5.1 Materials

Guinea pig brains, rat brains and rat livers were commercially available (Harlan-Winkelmann, Borchen, Germany). Pig brains were a donation of the local slaughterhouse (Coesfeld, Germany). The recombinant L(tk-) cells stably expressing the GluN2B receptor were obtained from Prof. Dr. Dieter Steinhilber (Frankfurt, Germany). Homogenizers: Elvehjem Potter (B. Braun Biotech International, Melsungen, Germany) and Soniprep® 150 (MSE, London, UK). Centrifuges: Cooling centrifuge model Eppendorf 5427R (Eppendorf, Hamburg, Germany) and High-speed cooling centrifuge model Sorvall® RC-5C plus (Thermo Fisher Scientific, Langenselbold, Germany). Multiplates: standard 96 well multiplates (Diagonal, Muenster, Germany). Shaker: self-made device with adjustable temperature and tumbling speed (scientific workshop of the institute). Harvester: MicroBeta® FilterMate 96 Harvester. Filter: Printed Filtermat Typ A and B. Scintillator: Meltilex® (Typ A or B) solid state scintillator. Scintillation analyzer: MicroBeta® Trilux (all Perkin Elmer LAS, Rodgau-Jügesheim, Germany).

4.5.2 Preparation of membrane homogenates from pig brain cortex

Fresh pig brain cortex was homogenized with the potter (500-800 rpm, 10 up and down strokes) in 6 volumes of cold 0.32 M sucrose. The suspension was centrifuged at 1,200 x g for 10 min at 4 °C. The supernatant was separated and centrifuged at 31,000 x g for 20 min at 4 °C. The pellet was resuspended in 5-6 volumes of TRIS/EDTA buffer (5 mM TRIS/1 mM EDTA, pH 7.5) and centrifuged again at 31,000 x g (20 min, 4 °C). The final pellet was resuspended in 5-6 volumes of buffer and frozen (-80 °C) in 1.5 mL portions containing about 0.8 mg protein/mL.

4.5.3 Preparation of membrane homogenates from rat liver

Two rat livers were cut into small pieces and homogenized with the potter (500-800 rpm, 10 up and down strokes) in 6 volumes of cold 0.32 M sucrose. The suspension was centrifuged at 1,200 x g for 10 min at 4 °C. The supernatant was separated and centrifuged at 31,000 x g for 20 min at 4°C. The pellet was resuspended in 5-6 volumes of buffer (50 mM TRIS, pH 8.0) and incubated at rt for 30 min. After the incubation, the suspension was centrifuged again at 31,000 x g for 20 min at 4 °C. The final pellet was resuspended in 5-6 volumes of buffer and stored at -80 °C in 1.5 mL portions containing about 2 mg protein/mL.

4.5.4 Cell culture and preparation of membrane homogenates for the GluN2B [47].

Mouse L(tk-) cells stably transfected with the dexamethasone-inducible eukaryotic expression vectors pMSG GluN1a, pMSG GluN2B (1:5 ratio) were grown in Modified Earl's Medium (MEM) containing 10 % of standardized FCS (Biochrom AG, Berlin, Germany). The expression of the NMDA receptor at the cell surface was induced after the cell density of the adherent growing cells had reached approximately 90 % of confluency. For the induction, the original growth medium was replaced by growth medium containing 4µM dexamethasone and 4µM ketamine (final concentration). After 24 h, the cells were rinsed with phosphate buffered saline solution (PBS, Biochrom AG, Berlin, Germany), harvested by mechanical detachment and pelleted (10 min, 5,000xg).

For the binding assay, the cell pellet was resuspended in PBS solution and the number of cells was determined using a Scepter® cell counter (MERCK Millipore, Darmstadt, Germany). Subsequently, the cells were lysed by sonication (4 C, 6x10s cycles with breaks of 10 s). The resulting cell fragments were centrifuged with a high performance cool centrifuge (23,500xg, 4 C). The supernatant was discarded and the pellet was resuspended in a defined volume of PBS yielding cell fragments of approximately 500,000 cells/mL. The suspension of membrane homogenates was sonicated again (4 °C, 2 x 10 s cycles with a break of 10 s) and stored at -80 °C.

4.5.5 Protein determination

The protein concentration was determined by the method of Bradford [65], modified by Stoscheck [66]. The Bradford solution was prepared by dissolving 5 mg of Coomassie Brilliant Blue G 250 in 2.5 mL of EtOH (95 %, v/v). 10 mL deionized H_2O and 5 mL phosphoric acid (85%, m/v) were added to this solution, the mixture was stirred and filled to a total volume of 50 mL with deionized water. The calibration was carried out using bovine serum albumin as a standard in 9 concentrations (0.1, 0.2, 0.4, 0.6, 0.8, 1.0, 1.5, 2.0 and 4.0 mg /mL). In a 96 well standard multiplate, 10 µL of the calibration solution or 10 µL of the membrane receptor preparation were mixed with 190 µL of the Bradford solution, respectively. After 5 min, the UV absorption of the protein-dye complex at λ = 595 nm was measured with a plate reader (Tecan Genios®, Tecan, Crailsheim, Germany).

4.5.6 General procedures for the binding assays

The test compound solutions were prepared by dissolving approximately 10 µmol (usually 2-4 mg) of test compound in DMSO so that a 10 mM stock solution was obtained. To obtain the required test solutions for the assay, the DMSO stock solution was diluted with the respective assay buffer. The filtermats were presoaked in 0.5 % aqueous polyethylenimine solution for 2 h at rt before use. All binding experiments were carried out in duplicates in the 96 well multiplates. The

concentrations given are the final concentration in the assay. Generally, the assays were performed by addition of 50 µL of the respective assay buffer, 50 µL of test compound solution in various concentrations (10^{-5}, 10^{-6}, 10^{-7}, 10^{-8}, 10^{-9} and 10^{-10} mol/L), 50 µL of the corresponding radioligand solution and 50 µL of the respective receptor preparation into each well of the multiplate (total volume 200 µL). The receptor preparation was always added last. During the incubation, the multiplates were shaken at a speed of 500-600 rpm at the specified temperature. Unless otherwise noted, the assays were terminated after 120 min by rapid filtration using the harvester. During the filtration, each well was washed five times with 300 µL of water. Subsequently, the filtermats were dried at 95 °C. The solid scintillator was melted on the dried filtermats at a temperature of 95 °C for 5 min. After solidifying of the scintillator at rt, the trapped radioactivity in the filtermats was measured with the scintillation analyzer. Each position on the filtermat corresponding to one well of the multiplate was measured for 5 min with the [^{3}H]-counting protocol. The overall counting efficiency was 20 %. The IC_{50} values were calculated with the program GraphPad Prism® 3.0 (GraphPad Software, San Diego, CA, USA) by non-linear regression analysis. Subsequently, the IC_{50} values were transformed into K_i values using the equation of Cheng and Prusoff [67]. The K_i values are given as mean value ± SEM from three independent experiments.

4.5.7 Performance of the binding assays

4.5.7.1 Ifenprodil binding site of GluN2B subunit containing NMDA receptors

The competitive binding assay was performed with the radioligand [^{3}H]ifenprodil (60 Ci/mmol; BIOTREND, Cologne, Germany). The thawed cell membrane preparation from the transfected L(tk-) cells (about 20 µg protein) was incubated with various concentrations of test compounds, 5 nM [^{3}H]-ifenprodil, and TRIS/EDTA-buffer (5 mM TRIS/1 mM EDTA, pH 7.5) at 37 °C. The non-specific binding was determined with 10 µM unlabeled ifenprodil. The K_d value of ifenprodil is 7.6 nM [47].

4.5.7.2 σ_1 receptor assay

The assay was performed with the radioligand [^{3}H]-(+)-pentazocine (22.0 Ci/mmol; Perkin Elmer). The thawed membrane preparation of guinea pig brain cortex (about 100 µg of the protein) was incubated with various concentrations of test compounds, 2 nM [^{3}H]-(+)-pentazocine, and TRIS buffer (50 mM, pH 7.4) at 37 °C. The non-specific binding was determined with 10 µM unlabeled (+)-pentazocine. The K_d value of (+)-pentazocine is 2.9 nM [68].

4.5.7.3 σ_2 receptor assay

The assays were performed with the radioligand [^{3}H]di-*o*-tolylguanidine (specific activity 50 Ci/mmol; ARC, St. Louis, MO, USA). The thawed rat liver membrane preparation (about 100 µg protein) was incubated with various concentrations of the test compound, 3 nM [^{3}H]di-*o*-tolylguanidine and buffer containing (+)-pentazocine (500 nM (+)-pentazocine in TRIS buffer (50 mM TRIS, pH 8.0)) at rt. The non-specific binding was determined with 10 µM non-labeled di-*o*-tolylguanidine. The K_d value of di-*o*-tolylguanidine is 17.9 nM [69].

4.6 Antioxidant assay

4.6.1 ABTS radical scavenging activity

The antioxidant activity of the compounds was tested from the bleaching of the green coloured ethanolic solution of ABTS [70]. To 1.8 mL of ethanolic solution of ABTS 7mM 200 µL of test compounds, each one diluted according the following concentration 0.05, 0.1, 0.2 and 0.4 mg/mL. These mixtures were incubated for 40 min at room temperature, then the absorbances were recorded at 735 nm against ABTS solution. The results were measured as the percent of inhibition (IC%) of ABTS radical, calculated by the following formula.

% IC = [(Abs ABTS - Abs Sample) / Abs ABTS] x 1

Tests were performed in triplicate and data were expressed ad mean value ± SEM.

The IC % was used to determine the IC_{50} values.

The ABTS method was applied also to measure the IC_{50} of Ascorbic acid, used as antioxidant compound comparing value.

4.6.2 Hydrogen peroxide radical scavenging activity

Four different concentrations of test compounds (0.05, 0.1, 0.2 and 0.4 mg/mL) were diluted in phosphate buffer (pH 7.4) [71]. Also, a solution of Hydrogen peroxide 4 mM was prepared in phosphate buffer and 0.353 mL of this solution were added to 2.0 mL of each solution of test compounds. The mixtures were measured at 239 nm. The percent of inhibition of free radical production from hydrogen peroxide was calculated using the above formula.

Tests were performed in triplicate and data were expressed ad mean value ± SEM

4.7 Cytotoxicity and neuroprotection assays

The human SH-SY5Y (neuroblastoma), HEP3B (hepatocarcinoma) and HeLa (cervical adenocarcinoma) cell lines were maintained in Dulbecco's modified Eagle's medium (DMEM) Glutamax (Life Technologies) supplemented with 10% (v/v) fetal bovine serum (FBS) and 1x

Antibiotic Antimycotic Solution (Sigma-Aldrich, 100 U penicillin, 100 μg/mL streptomycin and 0.25 μg/mL amphotericin B) at 37 °C in a humidified incubator with a 5%CO_2/95% air atmosphere. The cytotoxic effects of the dual σR/GluN2b ligands were evaluated by MTT test as previously described [43].

Briefly, SH-SY5Y cells were plated ($2x10^3$ cells/well) in 96-well plates 24 h prior to treatment with the compounds. The compounds were dissolved in DMSO and serially diluted in culture medium to achieve the desired final concentrations. The final concentration of DMSO in the culture medium was always = 1.0 %. After 48 h, 15 μl MTT solution (5 mg/mL, Sigma-Aldrich, St. Louis, MO, USA) was added to each well, and plates were incubated for 4 h at 37°C. Multiwell plates were then read in a iMark Microplate Absorbance Reader (Bio-rad). All compounds were assayed in triplicates, and the results are the average of at least three independent experiments. Results are presented by mean absorbance (A595 subtracted by A655) ± SEM. The statistical analysis was performed with GraphPad Prism 5 (GraphPad Software, Inc, La Jolla, CA, USA) software using an unpaired t-test. $P < 0.05$ was considered statistically significant.

For the neuroprotection assays, cells were seeded at $5x10^3$ in 96-well plates. After 24 h, the medium was aspirated and replaced with fresh medium containing the compounds at 25 μM. After 48 h, cells were treated with H_2O_2 1000 μM for 4 hrs. H_2O_2 was freshly prepared from a 30% stock solution prior to each experiment. Control cells without H_2O_2 treatment were included in all experiments.

Acknowledgment

We acknowledge the CINECA Awards N. HP10BTJPER, 2017, for the availability of high performance computing resources and support. The authors would like to thank Dr. Fabio Hollan (Dept. Of Chemistry and Pharmaceutical Sciences-Univ. of Trieste) for MS data.

References

1- M. Hanner, F.F. Moebius, A. Flandorfer, H.G. Knaus, J. Striessnig, E. Kempner, H. Glossmann, Purification, molecular cloning, and expression of the mammalian sigma1-binding site. Proc. Natl. Acad. Sci. U.S.A. 93 (1996) 8072-8077.

2- R. Kekuda, P.D. Prasad, Y.J. Fei, F.H. Leibach, V. Ganapathy, Cloning and functional expression of the human type 1 sigma receptor (hSigmaR1). Biochem. Biophys. Res. Commun. 229 (1996) 553−558.

3- S. B. Hellewell, A. Bruce, G. Feinstein, J. Orringer, W. Williams, W.D. Bowen, Rat liver and kidney contain high densities of σ1 and 2 receptors: characterization by ligand binding and photoaffinity labeling, Eur. J. Pharmacol., Mol. Pharmacol. Sect. 268 (1994) 9−18.

4- H.R. Schmidt, S. Zheng, E. Gurpinar, A. Koehl, A. Manglik, A.C. Kruse, Crystal structure of the human σ1 receptor, Nature 532 (2016) 527−530.

5- T. Hayashy, T.P. Su, Regulating ankyrin dynamics: Roles of sigma-1 receptors, Proc. Natl. Acad. Sci. U. S. A. 98 (2001) 491-496.

6- Z. Wu, W.D. Bowen, Role of sigma-1 receptor C-terminal segment in inositol 1,4,5-trisphosphate receptor activation: constitutive enhancement of calcium signaling in MCF-7 tumor cells, J. Biol. Chem. 283 (2008) 28198-28215.

7- E.J. Cobos, J.M. Entrena, F.R. Nieto, C.M. Cendan, E.D. Pozo, Pharmacology and therapeutic potential of sigma-1 ligands, Curr. Neuropharmocol. 6 (2008) 344-366.

8- T. Maurice, B.P. Lockhart, Neuroprotective and anti-amnesic potentials of sigma (sigma) receptor ligands, Prog. Neuropsychopharmacol. Biol. Psychiatry. 21(1997) 69-102.

9- M. King, Y.X. Pan, J. Mei, A. Chang, J. Xu, G.W. Pasternak, Enhanced kappa-opioid receptor-mediated analgesia by antisense targeting the sigma1 receptor, Eur. J. Pharmacol. 331 (1997) R5-6.

10- K.A. McCracken, W.D. Bowen, F.O. Walker, B. De Costa, R.R. Matsumoto, Two novel sigma receptor ligands, BD1047 and LR172, attenuate cocaine-induced toxicity and locomotor activity, Eur. J. Pharmacol. 370 (1999) 225-232.

11- S. Modell, D. Nober, R. Holzbach, Efficacy and safety of an opiate sigma-receptor antagonist (SL 82.0715) in schizophrenic patients with negative symptoms: an open dose-range study, Pharmacopsychiatry 29 (1996) 63-66.

12- M.T. Huber, U. Gotthardt, W. Schreiber, J.C. Krieg, Efficacy and safety of the sigma receptor ligand EMD 57445 (panamesine) in patients with schizophrenia: an open clinical trial, Pharmacopsychiatry 32 (1999) 68-72.

13- F.J. Kim, C.M. Maher, Sigma1 Pharmacology in the Context of Cancer. Handb Exp Pharmacol. 244 (2017) 237-308.

14- W.R. Martin, C.E. Eades, J.A. Thompson, R.E. Huppler, P.E. Gilbert, The effects of morphine- and nalorphine- like drugs in the nondependent and morphine-dependent chronic spinal dog, J. Pharmacol. Exp Ther. 197 (1976) 517–532.

15- A. Alon, H.R. Schmidt, M.D. Wood, J.J. Sahn, S.F. Martin, A.C. Kruse, Identification of the gene that codes for the σ2 receptor, Proc. Nat. Ac. Sc. 114 (2017) 7160–7165.

16- F. Bartz, L. Kern, D. Erz, M. Zhu, D. Gilbert, T. Meinhof, U. Wirkner, H. Erfle, M. Muckenthaler, R. Pepperkok, H. Runz, Identification of cholesterol-regulating genes by targeted RNAi screening, Cell. Metab.10 (2009) 63-75.

17- A. Riad, C. Zeng, C.C. Weng, H. Winters, K. Xu, M. Makvandi, T. Metz, S. Carlin, R.H. Mach, Sigma-2 Receptor/TMEM97 and PGRMC-1 Increase the Rate of Internalization of LDL by LDL Receptor through the formation of a Ternary Complex, Sc. Rep. 8 (2018) 16845.

18- M.A. Cahill et al. The emerging role of progesterone receptor membrane component 1 (PGRMC1) in cancer biology. Biochim. Bioph. Acta 1866 (2016) 339–349.

19- C. Zeng, J. Rothfuss, J. Zhang, W. Chu, S. Vanveravong, Z. Tu, F. Pan, K.C. Chang, R. Hotchkiss, R.H. Mach, Sigma-2 ligands induce tumor cell death by multiple signaling pathways, Br. J. Cancer. 106 (2012) 693–701.

20- W.D. Bowen, Sigma receptors: Recent advances and new clinical potentials. Pharma. Acta Helv. 74 (2000) 211-218.

21- D. Zamanillo, L. Romero, M. Merlos, J.M. Vela, Sigma 1 receptor: a new therapeutic target for pain. Eur. J. Pharmacol. 716 (2013) 78−93.

22- J.J. Sahn, G.L. Mejia, P.R. Ray, S.F. Martin, T.J. Price, Sigma 2 Receptor/Tmem97 Agonists Produce Long Lasting Antineuropathic Pain Effects in Mice", ACS Chem. Neurosci. 8 (2017) 1801-1811.

23- H. Kayed, J. Kleeff, J. Ding, J. Hammer, T. Giese, H. Zentgraf, M.W. Buchler, H. Friess, Expression analysis of MAC30 in human pancreatic cancer and tumors of the gastrointestinal tract. Histol. Histopathol. *19* (2004) 1021–1031.

24- K.Y. Han, X. Gu, H.R. Wang, D. Liu, F.Z. Lv, J.N. Li, Overexpression of MAC30 is associated with poor clinical outcome in human non-small cell lung cancer. Tumour Biol. 34 (2013) 821–825.

25- H. Ding, X.H. Gui, X.B. Lin, R.H. Chen, H.R. Cai, Y. Fen, Y.L. Sheng, Prognostic value of MAC30 expression in human pure squamous cell carcinomas of the lung, Asian Pac. J. Cancer Prev. 17 (2016) 2705–2710.

26- M. Xiao, H. Li, S. Yang, Y. Huang, S. Jia, H. Wang, J. Wang, Z. Li, Expression of MAC30 protein is related to survival and clinicopathological variables in breast cancer. J. Surg. Oncol. 107 (2013) 456–462.

27- S. Yang, H. Li, Y. Liu, X. Ning, F. Meng, M. Xiao, D. Wang, G. Lou, Y. Zhang, Elevated expression of MAC30 predicts lymph node metastasis and unfavourable prognosis in patients with epithelial ovarian cancer. Med. Oncol. 30 (2013) 324.

28- G. Qiu, W. Sun, Y. Zou, Z. Cai, P. Wang, X. Lin, J. Huang, L. Jiang, X. Ding, G. Hu, RNA interference against TMEM97 inhibits cell proliferation, migration, and invasion in glioma cells. Tumour Biol. 36 (2015) 8231–8238.

29- X.Y. Xu, L.J. Zhang, Y.Q. Yu, X.T., Zhang, W.J. Huang, X.C. Nie, G.Q. Song, Down-regulated MAC30 expression inhibits proliferation and mobility of human gastric cancer cells, Cell Physiol. Biochem. 33 (2014) 1359–1368.

30- K. Schmit, C. Michiels, TMEM Proteins in Cancer: A Review, Front Pharmacol. 9 (2018) 1345.

31- H. Husi, NMDA Receptors, Neural Pathways, and Protein Interaction Databases, Int. Rev. Neurobiol. 61 (2004) 49-77

32- S. Cull-Candy, S. Brickley, M. Farrant, NMDA receptor subunits: diversity, development and disease, Curr. Opin. Neurobiol. 11 (2001) 327–335.

33- M.H. Ulbrich, E.Y. Isacoff, Rules of engagement for NMDA receptor subunits, Proc. Natl. Acad. Sci. U S A 105 (2008) 14163–14168.

34- L. Mony, J. N. C. Kew, M. J. Gunthorpe, P. Paoletti, Br. J. Pharmacol. 157 (2009) 1301–1317.

35- J. Lewerenz, P. Maher, Chronic Glutamate Toxicity in Neurodegenerative Diseases—What is the Evidence?, Front. Neurosci. 15 (2015) 469.

36- G. Riedel, B. Platt, J. Micheau, Behav. Brain Res. 140 (2003) 1–47.

37- P. Paoletti, C. Bellone, Q. Zhou, NMDA receptor subunit diversity: impact on receptor properties, synaptic plasticity and disease, Nat. Rev. Neurosc. 14 (2013) 383-400.

38- I. J. Reynolds, R. J. Miller, Mol. Pharmacol. 36 (1989) 758–765.

39- A.S. Clemente, R. A. Nicoll, K.W. Roche, Diversity in NMDA receptor composition: many regulators, many consequences, Neuroscientists 19 (2013) 62-75.

40- E. Karakas, N. Simorowski, H. Furukawa, Crystal structure of amino terminal domain of NMDA receptor subunit GluN1, Nature 475 (2011) 249–253.

41- E. Karakas, H. Furukawa, Crystal Structure of GluN1a/GluN2B NMDA Receptor Ion Channel, Science 344 (2014) 992–997.

42- C.H. Lee, W. Lü, J.C. Michel, A. Goehring, J. Du, X. Song, E. Gouaux, NMDA receptor structures reveal subunit arrangement and pore architecture, Nature 511 (2014) 191-197.

43- D. Zampieri, L. Vio, M. Fermeglia, S. Pricl, B. Wünsch., D. Schepmann, M. Romano, M.G. Mamolo, E. Laurini, Computer-assisted design, synthesis, binding and cytotoxicity assessments of new 1-(4-(aryl(methyl)amino)butyl)-heterocyclic σ1 ligands, Eur. J. Med Chem. 121 (2016) 712–726.

44- M.G. Mamolo, D. Zampieri, C. Zanette, C. Florio, S. Collina, M. Urbano, O. Azzolina, L. Vio, Substituted benzylaminoalkylindoles with preference for the σ2 binding site, Eur. J. Med. Chem. 43 (2008) 2073-2081.

45- B. Wünsch, S. Thum, D. Schepmann, D.V. Kalinin, S.M. Ametamey, Replacement of benzylpiperidine moiety by fluorinated phenylalkyl side chains for the development of novel GluN2B receptor ligands, ChemMedChem, 13 (2018) 2522-2529.

46- E. Laurini, D. Zampieri, M.G. Mamolo, L. Vio, C. Zanette, C. Florio, P. Posocco, M. Fermeglia, S. Pricl, A 3D-pharmacophore model for σ2 receptors based on a series of substituted benzo[d]oxazol-2(3*H*)-one derivatives, Bioorg. Med. Chem. Lett. 20 (2010) 2954-2957.

47- D. Schepmann, B. Frehland, K. Lehmkuhl, B. Tewes, B. Wünsch, Development of a selective competitive receptor binding assay for the determination of the affinity to NR2B containing NMDA receptors, J. Pharm. Biomed. Anal. 53 (2010) 603–608.

48- T.T. Wager, X. Hou, P.R. Verhoest, A. Villalobos, Central nervous system multiparameter optimization desirability: application in drug discovery. ACS Chem. Nanosc., 7, (2016) 767-775.

49- C.A. Lipinski, Lead- and drug-like compounds: the rule-of-five revolution, Drug discovery today, Technologies 1 (2004) 337-341.

50- A.K. Malde, L. Zuo, M. Breeze, M. Stroet, D. Poger, P.c. Nair, C. Oostenbrink, A.E. Mark, An Automated Force Field Topology Builder (ATB) and Repository: Version 1.0. J. Chem. Theory Comput. 7 (2011) 4026-4037.

51- D.T. Ault, L.L. Werling, SH-SY5Y cells as a model for sigma receptor regulation of potassium-stimulated dopamine release, Brain Res. 877 (2000) 354-360.

52- N. Ismail, M. Ismail, M.U. Imam, N.H. Azmi, S.F. Fathy, J.B. Foo, M.F. Abu Kabar, Mechanistic basis for protection of differentiated SH-SY5Y cells by oryzanol-rich fraction against hydrogen peroxide-induced neurotoxicity, BMC Complement. Alt. Med. 14 (2014) 467.

53- Y.J. Choi, E.B. Kwak, J.W. Lee, I.Y. Cheong, H.J. Lee, S.S. Kim, M.J. Kim, Y.S. Kwon, W. Chun, Cytoprotective Effects of Docosyl Cafferate against tBHPInduced Oxidative Stress in SH-SY5Y Human Neuroblastoma Cells, J. Biomed. Biotechnol. (2010) Article ID 803815, doi:10.1155/2010/803815

54- T.F. Beckhauser, J. Francis-Oliveira, R. De Pasquale, Reactive Oxygen Species: Physiological and Physiopathological Effects on Synaptic Plasticity, J. Exp. Neurosci. 10 (2016) 23-48.

55- A. Garcimartin, J.J. Merino, M.P. González, M.I. Sánchez-Reus, F.J. Sánchez-Muniz, S. Bastida, J. Benedí, Organic silicon protects human neuroblastoma SH-SY5Y cells against hydrogen peroxide effects, BMC Complement Altern. Med. 14 (2014) 384.

56- J. Chetsawang, P. Govitrapong, B. Chetsawang, Hydrogen peroxide toxicity induces Ros signaling in human neuroblastoma SH-SY5Y cultured cells, J. Biomed. Biotechnol. (2010) Article ID: 803815, doi: 10.1155/2010/803815.

57- G.M. Grunewald, V.H. Dahanukar, T.M. Caldwell, K.R. Criscione, Examination of the Role of the Acidic Hydrogen in Imparting Selectivity of 7-(Aminosulfonyl)-1,2,3,4-tetrahydroisoquinoline (SK&F 29661). Toward Inhibition of Phenylethanolamine N-Methyltransferase vs the α2-Adrenoceptor 1a, J. Med. Chem. 40 (1997) 3997-4005.

58- A. Waterhouse, M. Bertoni, S. Bienert, G. Studer, G. Tauriello, R. Gumienny, F.T. Heer, T.A.P. de Beer, C. Rempfer, L. Bordoli, R. Lepore, T. Schwede, SWISS-MODEL: homology modelling of protein structures and complexes. Nucleic acids res. 46 (2018) W296-W303.

59- J.J.P. Stewart, MOPAC A semiempirical molecular-orbital program, J. Comput. Aided Mol. Des. 4 (1990) 1-45.

60- O. Trott, A.J. Olson, AutoDock Vina: improving the speed and accuracy of docking with a new scoring function, efficient optimization, and multithreading. J. comput. chem. 31 (2010) 455-461.

61- R.A. Laskowski, M.B. Swindells, LigPlot+: multiple ligand–protein interaction diagrams for drug discovery, J. Chem. Inf. Mod. 51 (2011) 2778-2786.

62- B. Hess, H. Bekker, H.J.C. Berendsen, J.G.E.M. Fraaije, LINCS: a linear constraint solver for molecular simulations. J. Comput. Chem. 18 (1997) 1463-1472.

63- S. Pronk, S. Páll, R. Schulz, P. Larsson, P. Bjelkmar, R. Apostolov, M.R. Shirts, J.C. Smith, P.M. Kasson, D. van der Spoel, B. Hess, E. Lindahl, GROMACS 4.5: a high-throughput and highly parallel open source molecular simulation toolkit. Bioinf. 29 (2013) 845-854.

64- R. Kumari, A.M. Lynn, g_mmpbsa, • a GROMACS tool for high-throughput MM-PBSA calculations. J. chem. inf. model. 54 (2014) 1951-1962.

65- M.M. Bradford, A Rapid and sensitive Method for the Quantitation of Microgram Quantities of Protein Utilizing the Principle of Protein-Dye Binding, Anal. Biochem. 72 (1976) 248–254.

66- C. Stoscheck, Quantification of Protein, Methods in Enzymology, 182 (1990) 50–68.

67- Y.C. Cheng, W.H. Prusoff, Relationship between the inhibition constant (KI) and the concentration of inhibitor which causes 50 per cent inhibition (I50) of an enzymatic reaction, Biochem. Pharmacol. 22 (1973**)** 3099–3108.

68- D.L. DeHaven-Hudkins, L.C. Fleissner, F.Y. Ford-Rice, Characterization of the binding of [3H](+)-pentazocine to σ recognition sites in guinea pig brain, Eur. J. Pharmacol.: Molecular Pharmacology 1227 **(**1992**)** 371–378.

69- R.H. Mach, C.R. Smith, S.R. Childers, Ibogaine possesses a selective affinity for σ2 receptors, Life Sciences 57 (1995) PL57–PL62.

70- R. Re, N. Pellegrini, A. Proteggente, A. Pannala, M. Gang, C. Rice, Antioxidant activity applying an improved ABTS radical cation decolorization assay. Free radical biology & medicine (1999), 26(9), 1231-1237.

71- D.Ashok, S. Gundu, V.K. Aamate, M.G. Devulapally, Conventional andmicrowave-assisted synthesis of new indole-tethered benzimidazole-based 1,2,3-triazoles and evaluation of their antimycobacterial, antioxidant and antimicrobial activities, Mol. Divers. 22 (2018) 769-778.

Highlights:

1. New hybrid derivatives as dual σR/GluN2b ligands were designed and synthesized
2. Some of new derivatives showed pan-affinity for the sigma receptor
3. *In silico* affinity evaluation confirmed the experimental data
4. We evaluated the neuroprotective activity of the most interesting derivatives
5. Compounds **24** and **28** displayed the best biological profile.